

See discussions, stats, and author profiles for this publication at: <https://www.researchgate.net/publication/393370653>

Late Cretaceous (Cenomanian–Coniacian) Stage of Rifting in the Northern Part of the North Atlantic and Arctic Basin

Article in *Geotectonics* · July 2025

DOI: 10.1134/S0016852125700098

CITATIONS

0

READS

6

2 authors, including:



[A. V. Soloviev](#)

Russian Academy of Sciences

122 PUBLICATIONS 1,083 CITATIONS

[SEE PROFILE](#)

Late Cretaceous (Cenomanian–Coniacian) Stage of Rifting in the Northern Part of the North Atlantic and Arctic Basin

A. V. Zayonchek^a and A. V. Soloviev^{a, b, *}

^a *Geological Institute, Russian Academy of Sciences, Moscow, 119017 Russia*

^b *All-Russian Research Geological Oil Institute, Moscow, 105118 Russia*

**e-mail: soloviev@vnigni.ru*

Received October 13, 2023; revised December 26, 2024; accepted March 6, 2025

Abstract—Apatite fission track dating of Triassic (Anisium–Norium) sandstones of the Severnaya borehole on Graham Bell Island of Franz Josef Land was performed. The Late Cretaceous age (~90 Ma) of the transition from the stage of relative temperature and tectonic stability to the stage of “rapid” rock exhumation has been established. The Late Cretaceous (Cenomanian–Cognacian) stage of rock exhumation is widely manifested in the Arctic Basin and its frame and correlates with the stage of magmatism. It is suggested that these events record one of the stages of rifting development in the northern part of the North Atlantic and Arctic Basin, which is associated with reorganization of the direction of plate movement in the North Pacific Ocean.

Keywords: Arctic Basin, geodynamics, thermogeochronological studies, apatite fission track dating (AFT), magmatism, Cretaceous rifting

DOI: 10.1134/S0016852125700098

INTRODUCTION

The Arctic Ocean contains the Amerasian and Eurasian deep-water basins separated by the Lomonosov Ridge. According to most geologists and geophysicists, the Eurasian basin was formed in the Cenozoic as a result of the sliding of the North American, including the Lomonosov Ridge, and Eurasian lithospheric plates [6, 15, 48, 88] (Fig. 1).

The boundary of the North American and Eurasian plates is the mid-ocean Gakkel Ridge, which in the east can be traced to the Laptev Sea, which is a rift-related continuation of the Eurasian Basin [12].

In the Paleocene–Early Oligocene, the Greenland Plate existed independently between the North American and Eurasian plates, which moved in a westerly direction during the Paleocene, which led to compression of the northeastern part of Greenland and Western coast of Svalbard [138, 144, 151].

At the Paleocene–Eocene boundary, there was a sharp change in the direction of movement of the Greenland Plate to the northwest, which was the reason for folding (Yurikan orogeny) manifested on the Queen Elizabeth Islands of the Canadian Arctic Archipelago, on the northern and northeastern margins of Greenland and on Svalbard [138, 151, 159].

In the last decade, study of the stages of the Yurikan orogeny has been largely based on thermogeochronological studies in northeast Greenland, the northern Canadian Arctic Archipelago, and Svalbard (Fig. 1).

Comprehensive studies of the northwestern part of Svalbard established several stages of rock exhumation in the Cenozoic. It was revealed that exhumation of the complexes began in the Late Cretaceous ~88 Ma, long before the separation of the northeastern part of Greenland from the northwestern part of Svalbard [66, 67].

Similar results (~90 Ma) were previously obtained for Bear Island, which is located south of Svalbard [167]. On the eastern and northeastern coast of Greenland, a Late Cretaceous (~95–90 Ma) stage of rock exhumation was recorded, similar to the results for the southwest coast of Ellesmere Island (~90 Ma) [101, 109, 110].

Thermogeochronological studies of rock samples taken from the slope of the Lomonosov Ridge opposite the western part of Franz Josef Land, a cooling phase was established that began in the Late Cretaceous (~95 Ma) and is associated exhumation of sediments [119]; similar research was conducted on the western coast of the New Siberian Islands, in structures of the northern Verkhoyansk fold–thrust belt, the Pri-Verkhoyansk marginal trough; the data obtained recorded a stage of similarly aged rock cooling (~90 Ma) [4, 148].

Such similarity of the obtained data about age of cooling rocks allow us to identify the stage (95–90 Ma) of development of rifting from the North Atlantic to the Arctic Basin.

The aim of this article is to clarify this assumption, for which we have carried out thermogeochronological studies, using the apatite fission track dating (AFT), of

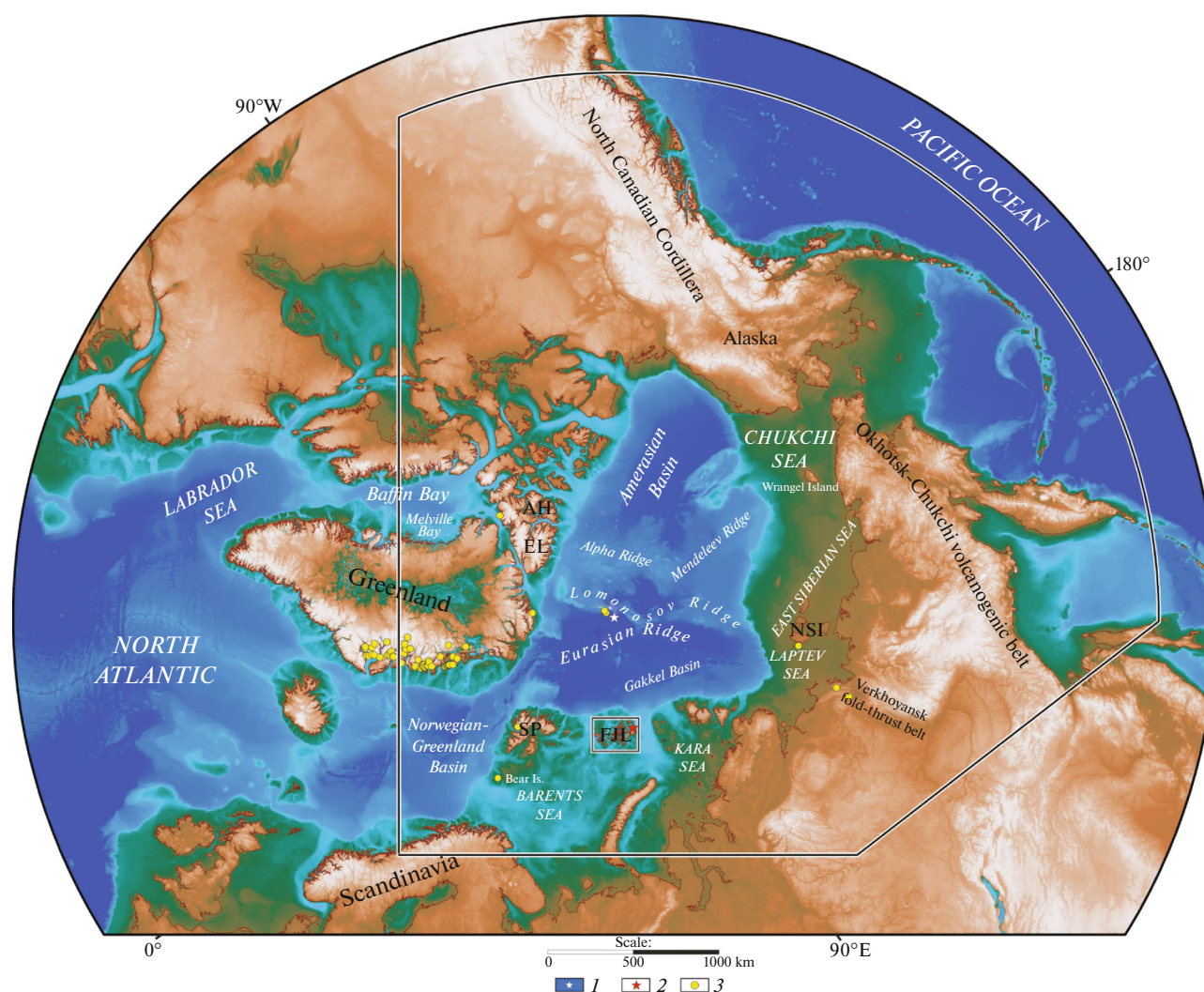


Fig. 1. Established Late Cretaceous (Cenomanian–Coniacian) manifestations of rock exhumation with age of 95–88 Ma in western sector of Arctic (data from [4, 66, 67, 101, 109, 110, 118, 147, 167], modified). Digital relief base IBCAO v.4 (according to [111]). Notation: AH, Axel Heiberg Island; FJL, Franz Josef Land; NI, New Siberian Islands; SZ, Severnaya Zemlya; SV, Svalbard; EL, Ellesmere Island. 1, North Pole; 2, position of Severnaya borehole Graham Bell Island; 3, rock exhumation points 95–88 Ma.

rock samples from the Severnaya borehole, located on the northeastern coast of Franz Josef Land.

GEOLOGICAL STRUCTURE OF FRANZ JOSEF LAND

Franz Josef Land is located on a rise of the marginal shelf that formed in the Mesozoic–Cenozoic in the north of the Barents–Kara Plate and is one of the key objects for studying the geological history of the Arctic Ocean. Franz Josef Land hosts Mesozoic (Triassic–Cretaceous) terrigenous deposits of marine, shallow-marine, and continental genesis [11, 13, 14, 59, 60].

Most of the area (~85%) of Franz Josef Land is under an ice sheet, which complicates research for Graham Bell Island, and prevents accurate lithostratigraphic correlation of Jurassic–Cretaceous deposits within the archipelago [13, 14, 18, 30] (Fig. 2).

The Triassic deposits have been studied much better (all three sections of the Triassic with division of the sections into stages and substages) with a total thickness of ~5 km, uncovered by the parametric Nagurskaya, Hayes, and Severnaya boreholes [3, 8, 27, 60]. The Triassic strata comprise lagoonal–marine and marine deposits in the lower part and predominantly lagoonal and continental deposits in the upper part [26, 60].

In the Mesozoic, Franz Josef Land was characterized by widespread mafic magmatism associated with the High Arctic Igneous Province (HALIP) [1, 9, 13, 14, 16, 17, 35, 37, 58–60, 95, 145].

Igneous formations of the trap (dolerite–basalt) formation are represented by flood basalts, flows, sills, dikes, and vent facies of volcanic apparatuses [17, 35] (Fig. 1). The dikes extend for tens of kilometers to the northwest and have a thickness from 1–2 to 20–25 m.

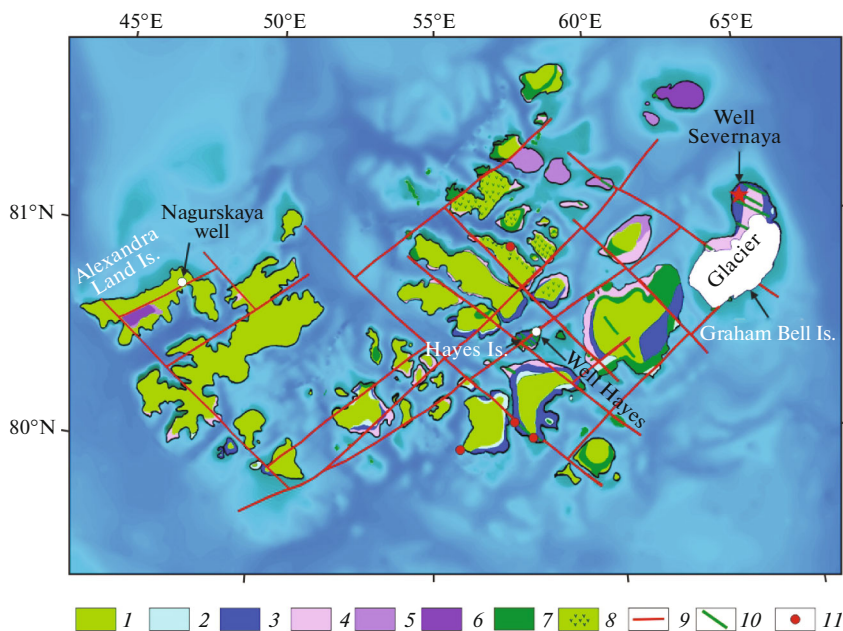


Fig. 2. Geological sketch map of Franz Josef Land (according to [35], modified). Digital relief base IBCAO v.4 (according to [111]): 1–6, sediments: 1, volcanic K_1 ; 2, marine terrigenous J_{2-3} ; 3, continental and shallow-marine J_1 ; 4, shallow-water marine T_3 ; 5, marine terrigenous T_2 ; 6, shallow-water marine T_1 ; 7, intrusive formations K_1 ; 8, zone of distribution of complex is moderate alkaline basalts–andesite–basalts; 9, major faults; 10, basic parallel dike complexes (not to scale); 11, central-type volcanic apparatuses.

The dike contacts are almost vertical. Layered intrusions (sills) with thicknesses from 20–30 to 100 m are regionally distributed and make up ~10% of the thickness of the terrigenous section.

Two main models of the evolution of basaltoid magmatism in Franz Josef Land have been developed:

- a short-term, one-stage formation of a large igneous province at the beginning of the Cretaceous [1, 9, 58, 145];

- the action of a long-lived (from the beginning of the Jurassic to the Early Cretaceous, inclusive) hot spot with several short pulses of igneous activation [36, 37].

Igneous bodies are exposed in sections of the Nagurskaya, Hayes, and Severnaya boreholes on Franz Josef Land [60]. Results of studies of catagenetic transformations of organic matter based on vitrinite reflectivity measurements, the pyrolytic characteristics of kerogen, and chromatograph mass spectrometric study of the composition and distribution of hydrocarbon molecular markers showed a high degree of organic matter conversion in sedimentary rocks near exposed igneous bodies [7, 25, 71]. Thus, there are limitations on the selection of samples from borehole cores for thermogeochronological studies.

Alexandra Land and Hayes Island, on which the Nagurskaya and Hayes boreholes were drilled, are characterized by the largest number of flood basalts, sills, and dikes [13, 14, 33, 57]:

- 20 or more intrusions of basic composition with a thickness of 2 to 140 m were identified in the Nagurskaya borehole section [13, 57];

- nine intrusions with a thickness from a few to ~60 m were identified in the Hayes borehole section [13, 14, 35].

There are a minimum of 6 intrusions for the Severnaya borehole on Graham Bell Island; therefore the Severnaya borehole is the most informative for thermogeochronological studies.

SAMPLING FROM THE SEVERNAYA BOREHOLE AND CORE PREPARATION

The Severnaya borehole was drilled between December 1977 and January 1979 by the Arctic oil exploration expedition of the Yaroslavlneftegazrazvedka trust (currently, JSC NPC Nedra, Yaroslavl, Russia).

From a total depth of 3523 m with core sampling, ~537 m (~15% of the depth) was passed with linear core removal of ~312 m. In the section of the parametric borehole, only Upper and Middle Triassic deposits are observed, although the lower, paleontologically uncharacterized horizons may belong to the Lower Triassic (Fig. 3).

The lithostratigraphic subdivision of the borehole section was carried out in a number of studies, which, however, had no significant differences [3, 8, 13, 27, 72]. In the Upper Triassic strata, clayey–silty deposits of the Norian Stage and predominantly sandy–silty deposits of the Carnian Stage with interlayers of carbonaceous rocks and coal lenses are distinguished. In the Middle Triassic strata, silty–clayey varieties of the Ladinian and Anisian stages predominate.

Table 1. Sandstone samples for apatite fission track dating from Severnaya borehole core

| Sample | Depth, m | Age ⁽ⁱ⁾ | Age ⁽ⁱⁱ⁾ , Ma | R ₀ ⁽ⁱⁱⁱ⁾ | T ^(iv) , °C | Track analysis method ^(v) |
|--------|----------|-----------------------------------|--------------------------|---------------------------------|------------------------|--------------------------------------|
| SEV1 | 633.5 | T _{3n2} (Upper Norian) | 218–208.5 | 0.42 | 13.0 | EDM |
| SEV1A | 650.6 | T _{3n2} (Upper Norian) | 218–208.5 | 0.43 | 13.5 | FT-U/Pb LA-ICP-MS |
| SEV2 | 782.0 | T _{3n1} (Lower Norian) | 227–218 | 0.53 | 15.5 | EDM |
| SEV3 | 1040.4 | T _{2c2} (Upper Carnian) | 230–227 | 0.92 | 20.5 | FT-U/Pb LA-ICP-MS |
| SEV4 | 1040.9 | T _{2c2} (Upper Carnian) | 230–227 | 0.92 | 20.5 | EDM |
| SEV5 | 1428.3 | T _{2c2} (Lower Carnian) | 237–230 | 0.57 | 28.0 | EDM |
| SEV6 | 2073 | T _{2l2} (Upper Ladinian) | 239–237 | 1.05 | 48.0 | EDM |
| SEV7 | 2689 | T _{2a2} (Upper Anisian) | 245–242 | 1.20 | 70.0 | EDM |

⁽ⁱ⁾ Age of rocks (according to [72]);

⁽ⁱⁱ⁾ age interval [57] used for thermal modeling;

⁽ⁱⁱⁱ⁾ R₀, reflectivity of vitrinite (according to [7]);

^(iv) T°C, current temperature according to logging data;

^(v) EDM, external detector method; FT-U/Pb LA-ICP-MS, combined track and U/Pb LA-ICP-MS dating.

U/Pb LA-ICP-MS dating of detrital zircon from four core samples showed that the main source of detrital material for the North Barents Sea sedimentary basin in the Middle–Late Triassic were rocks of the Ural fold belt [33] (Fig. 3). The main degradation took place from south and southeast.

The parametric borehole intersected six intrusive bodies from 3 to 87 m (Fig. 3).

Igneous rocks are represented by dolerites, microdolerites, micropegmatite gabbro, and olivine gabbro–dolerites [8]. A wide age range of intrusion formation from ~133 to 60 Ma was obtained using the K–Ar method [9, 36, 60].

U/Pb determinations from zircons and baddeleyite obtained for an 85-m-thick sill showed an age of 122.7 ± 0.3 Ma, which agrees with the concept of a short-term, single-stage eruption at the beginning of the Cretaceous [1, 58, 145].

Results of studies of catagenetic conversion of organic matter based on vitrinite reflectivity measurement data and the pyrolytic characteristics of kerogen showed a high degree of transformation of organic matter into sedimentary rocks located in the depth range of 940–1030 m (Fig. 3) [7, 71].

Drilling data in this the depth interval show that not igneous objects were exposed, but it is possible that an igneous body (dike (?)) is located near the wellbore. This assumption is confirmed by chromatography–mass spectrometric study of the distribution of hydrocarbon molecular markers, which showed a high degree of conversion of organic matter in sedimentary rocks [23].

Therefore, in the discussed depth interval of 940–1030 m, for our research, two sandstone samples were recovered (SEV3, SEV4) from depths below 1030 m (Fig. 3).

APATITE FISSION TRACK DATING OF SAMPLES FROM THE SEVERNAYA BOREHOLE CORE

Eight sandstone core samples from the Severnaya borehole (Graham Bell Island, Franz Josef Land) were recovered from different depth and stratigraphic levels to isolate monomineralic apatite fractions (Table 1, Fig. 3).

The use of AFT to reconstruct the thermal history of sediments associated with subsidence and exhumation is based on the fact that ²³⁸U fission tracks are formed at an almost constant rate and initial track length [91, 149].

In apatite, all fission tracks are completely annealed at temperatures above ~110°C and, partially, in the partial annealing zone in the range temperatures from ~60 to ~110°C [74, 93, 99]. Below temperatures of ~60°C, fission tracks in apatite are stable and anneal very slowly [84].

Apatite from six samples was dated using the external detector method at Stanford University (Stanford, California, USA) (analyst A.V. Soloviev); apatite from two samples was dated using a combined method of track and U/Pb LA-ICP-MS dating at GeoSep Services ((GSS), Moscow, Idaho, USA) (analyst Paul O’Sullivan). The HeFTy program was used to model the thermal history of deposition using track data v.1.8.0.64 [117].

Laboratory Methods of Trace Analysis

Monofractions of accessory apatites from core sandstones were analyzed at the laboratory of mineralogical and track analysis of the Geological Institute, Russian Academy of Sciences (Moscow, Russia) (analyst T.B. Afonina) using standard density and magnetic separation methods.

External detector method. We dated apatite grains from six core samples, SEV1, SEV2, SEV4, SEV5, SEV6, SEV7 (Tables 2, 3). The apatite samples were etched for 20 s in nitric acid (HNO_3), corresponding to the highest degree of nitrogen oxidation (5) at $T = 20^\circ\text{C}$. Dating of apatite grains was carried out using muscovite as a detector. Samples were irradiated in the Mark II TRIGA reactor at Oregon State University (OSU), Corvallis, Oregon, USA.

CN5 dosimetric glasses with muscovite external detectors were used as neutron flux monitors. External detectors were etched in a 48% solution of hydrofluoric acid (HF). Track counting was performed on a Zeiss Axioskop microscope (Carl Zeiss AG, Oberkochen, Germany) with a $100\times$ objective, $1.25\times$ tube factor, $10\times$ eyepieces, in transmitted reflected light on a Kinetek automated table (Kinetek, Stanford, California, USA) [73].

Dating of apatite grains was carried out only with the c axes, subparallel planes of the glass slide. Age was calculated using a Zeta calibration factor of 327.6. The track lengths were measured only in apatite grains with the axes subparallel to the plane of the slide, and only horizontal tracks were measured (within $\pm 5^\circ$ – 10°) according to the protocols [62, 124]. The length of the tracks was measured using a computer tablet and a tube calibrated with a micrometer [73]. The angles of inclination of the tracks to the c axis and track section dimensions D_{par} were also measured according to the protocols [117].

Combined track and U/Pb LA-ICP-MS dating [103]. We dated apatite grains from two core samples, SEV1A, SEV3, by sample processing and analysis [63] (Table 4).

Preparing blocks with apatite, spontaneous fission track counting and horizontal track length measurement were performed with unpolarized light at $2000\times$ magnification.

Isotopic ratio measurements in apatite for age determination were performed using an Element-2 mass spectrometer (ThermoFinnigan, San José, California, USA).

Analysis of Track Dating Data

To reconstruct the thermal history of sedimentary rocks using apatite track dating, eight sandstone samples were collected from deposits ranging in age from the Middle (Anisian) to the Late (Norian) Triassic (depths from 633.5 to 2689 m) (Fig. 3, Table 1).

Track ages of apatite (230 Ma and older) from samples SEV1 and SEV1A collected from depths above ~ 700 m, older than the age of the sampled deposits (Late Triassic, Late Norian), thus, the apatite did not experience track annealing. This means that this part of the section was not exposed to paleotemperatures (~ 80 – 120°C) after sedimentation.

Track age of apatite from samples collected below ~ 700 m (Middle and Late Triassic), younger than ~ 190 Ma, tracks in apatite have undergone annealing.

The track age of apatite decreases consistently with increasing core sampling depth (Fig. 4).

The graph of the distribution of apatite track ages of has a classical form, characteristic of an exhumed partial annealing zone.

The sharp change in slope of line on graph distributions ages shows a transition (~ 90 Ma) from a stage of relative temperature and tectonic stability to a stage of exhumation at a higher rate (steep slope) [85, 86] (Fig. 4).

Interpretation of track ages of apatite from borehole Northern showed that Middle and Upper Triassic deposits were located within the partial annealing zone (~ 80 – 120°C) in the Jurassic–Early Cretaceous, and exhumation accelerated in the Late Cretaceous (~ 90 Ma) (Fig. 4).

Track data allow a preliminary estimate of the exhumation rate in the Late Cretaceous of ~ 75 m/Ma (between 90 and 70 Ma).

Based on simulation using HeFTy 1.8.0.64 [117] data from track dating of apatite from the Severnaya borehole suggests that the Middle–Upper Triassic section was buried prior to the maximum (possibly close

Fig. 3. Fragment of section of Severnaya borehole (Franz Josef Land). Legend (Roman numerals): (I) lithostratigraphic section (along [27, 33, 71, 72]); (II) position of rock sampling (Sand. Ap, sandstone samples selected for apatite track dating, Sand. U–Pb, age (Ma) of detrital zircon grains from sandstone samples (according to [33]); Dol. (K–Ar), age (Ma) of samples from dolerite sills (according to [60, 96]); Dol. U–Pb, age (Ma) of zircons and baddeleyite from sill images dolerites (according to [58])); (III) results of vitrinite reflectivity measurements (R_{vt}^0) (according to [7, 71]) and trend line of degree of transformation of organic matter; (IV) measurement results $T_{\text{max}}^\circ\text{C}$ by Rock-Eval (according to [7, 71]); (V) current temperature curve (logging). 1–4, rocks: 1, argillites, 2, sandstones, 3, siltstones, 4, erupted; 5–6, cement type: 5, calcite, 6, dolomite; 7–12, rock textures: 7, layered; 8, cross-oblique; 9, tuberosity-cross oblique; 10, traces of bioturbation; 11, load texture, 12, ripple signs; 13, fauna; 14, plant detritus; 15, plant residues; 16–17, nodules: 16, pyrite; 17, siderite; 18, mica; 19, coal; 20, position and numbers of samples selected for apatite fission track dating; 21, position of sandstone samples for which age of detrital zircon grains was determined; 22–23, position of sill samples for which age was determined by: 22, K–Ar; 23, U–Pb (zircons and baddeleyite); 24, position of samples of vitrinite reflectivity measurements (R_{vt}^0) used to calculate trend of degree of transformation of organic matter; 25, position of vitrinite reflectivity measurements of samples (R_{vt}^0) not used to calculate trend of degree of transformation of organic matter; 26, position of measurement of samples $T_{\text{max}}^\circ\text{C}$ by Rock-Eval (according to [7, 71]); 27–32, stages of transformation of organic matter: PC, protocatagenesis; MC, mesocatagenesis (according to [7]): 27, PC₁; 28, MC₁; 29, MC₂; 30, MC₃; 31, MC₄; 32, MC₅.

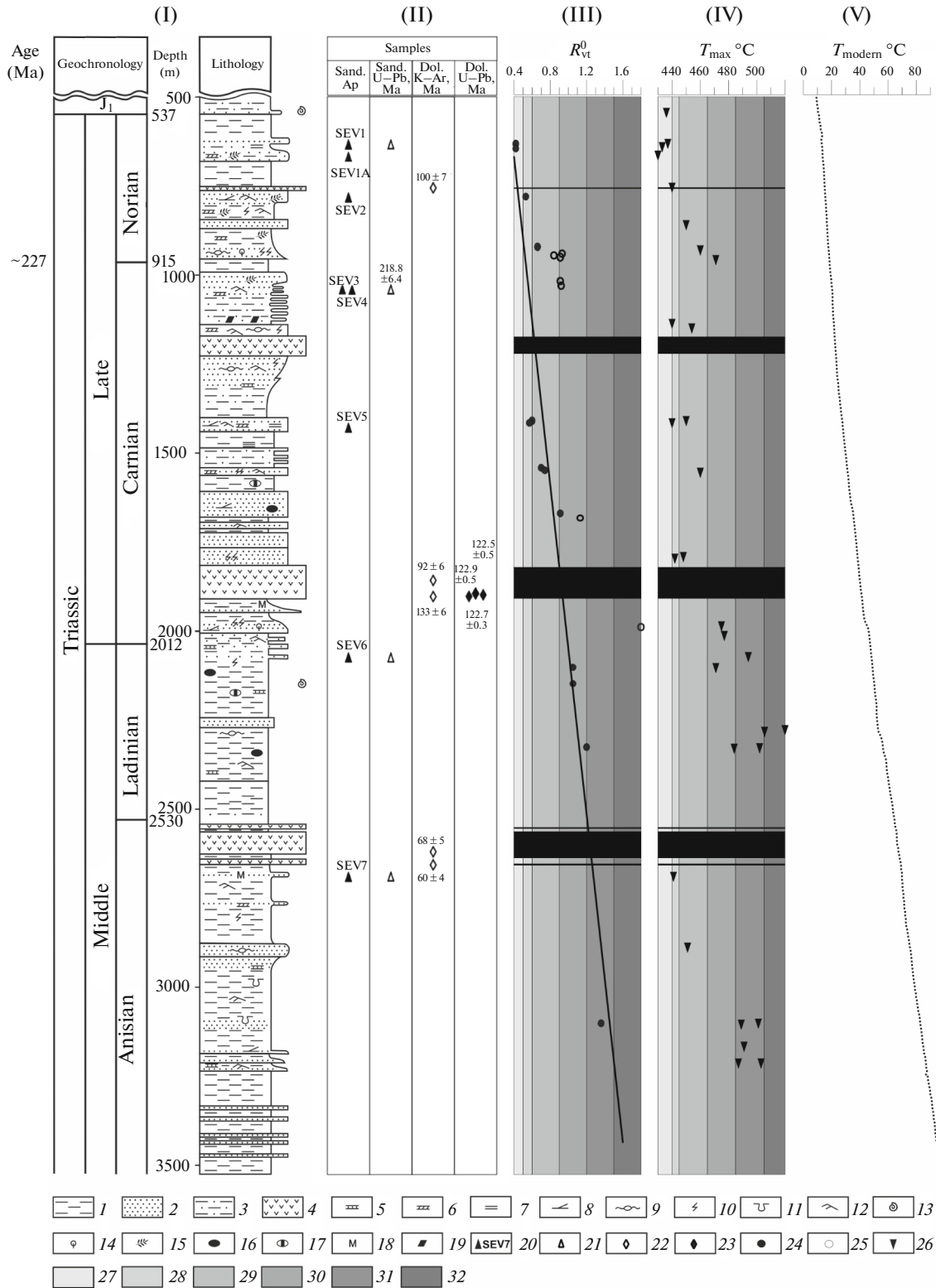


Table 2. Data on track age and length in apatite from Severnaya borehole core obtained by EDM

| Sample | Depth, m | Zircon grains, no. | Spontaneous division tracks | | Induced division tracks | | $P(\chi^2)$, % | Dosimeter | | Age, Ma | Error $\pm 1\sigma$, Ma | Tracks (no. length) | Average track length, μm | Error $\pm 1\sigma$, μm | Std _{dev} , μm | Interval D_{par} , μm |
|--------|----------|--------------------|-----------------------------|-------|-------------------------|-------|-----------------|-----------|-------|---------|--------------------------|---------------------|-------------------------------------|-------------------------------------|------------------------------------|---|
| | | | ρ_s | N_s | ρ_i | N_i | | ρ_d | N_d | | | | | | | |
| SEV1 | -633.5 | 20 | 1.4038 | 595 | 1.2080 | 512 | 97.7 | 1.282 | 3947 | 239.7 | 17.3 | 100 | 12.71 | 0.10 | 0.99 | 1.66-2.33 |
| SEV2 | -782 | 20 | 1.2990 | 447 | 1.4384 | 495 | 15.7 | 1.282 | 3947 | 185.9 | 16.7 | 57 | 12.39 | 0.13 | 1.02 | 1.73-2.68 |
| SEV4 | -1040.9 | 20 | 0.9765 | 972 | 1.8243 | 1816 | 34.8 | 1.310 | 3947 | 115.5 | 7.0 | 100 | 13.05 | 0.10 | 0.98 | 1.66-2.58 |
| SEV5 | -1428.3 | 17 | 1.2717 | 628 | 2.6183 | 1293 | 0.5 | 1.339 | 3947 | 109.0 | 8.9 | 102 | 12.46 | 0.10 | 1.06 | 1.69-3.12 |
| SEV6 | -2073 | 20 | 1.1183 | 412 | 3.3087 | 1219 | 15.0 | 1.339 | 3947 | 74.9 | 5.9 | 90 | 11.04 | 0.14 | 1.33 | 1.51-2.29 |
| SEV7 | -2689 | 20 | 0.9727 | 469 | 2.7978 | 1349 | 25.8 | 1.367 | 3947 | 77.6 | 5.3 | 88 | 11.52 | 0.14 | 1.34 | 1.73-2.89 |

Samples were irradiated with a thermal neutron flux of $\sim 8 \times 10^{15}$ neutron/cm² (Mark II TRIGA reactor) at Oregon State University (Corvallis, Oregon, USA);

Age standards and glass dosimeter with a known content were irradiated simultaneously with uranium samples (CN-1 for apatite);

when counting tracks, the following were used: a Zeiss Axioskop microscope (Carl Zeiss AG, Oberkochen, Germany) with automated system and digital tablet; maximum magnification 1562.5 \times ;

dry method, where ρ_s is the density of spontaneous fission tracks, N_s is the number of spontaneous fission tracks counted, ρ_i is the density of induced fission tracks of ^{235}U in the external detector in muscovite ($\times 10^6$ tracks per cm²), N_i is the number of counted induced division tracks, $P(\chi^2)$ is the probability χ^2 (by [89, 98]), ρ_d is the density of induced fission tracks in the external detector adjacent to the dosimeter glass ($\times 10^6$ tracks per cm²);

N_d is the number of tracks counted when determining ρ_d ;

no. lengths, number of measured track lengths;

Std_{dev}, standard deviation of track length distribution;

interval D_{par} , range of D_{par} values measured in all dated crystals and in all crystals in which track lengths were measured (according to [117]);

average age (according to [90]) was calculated using the Z-calibration method, Zeta - 327.6 (according to [106]) at Stanford University (Stanford, California, USA) (analyst A.V. Soloviev).

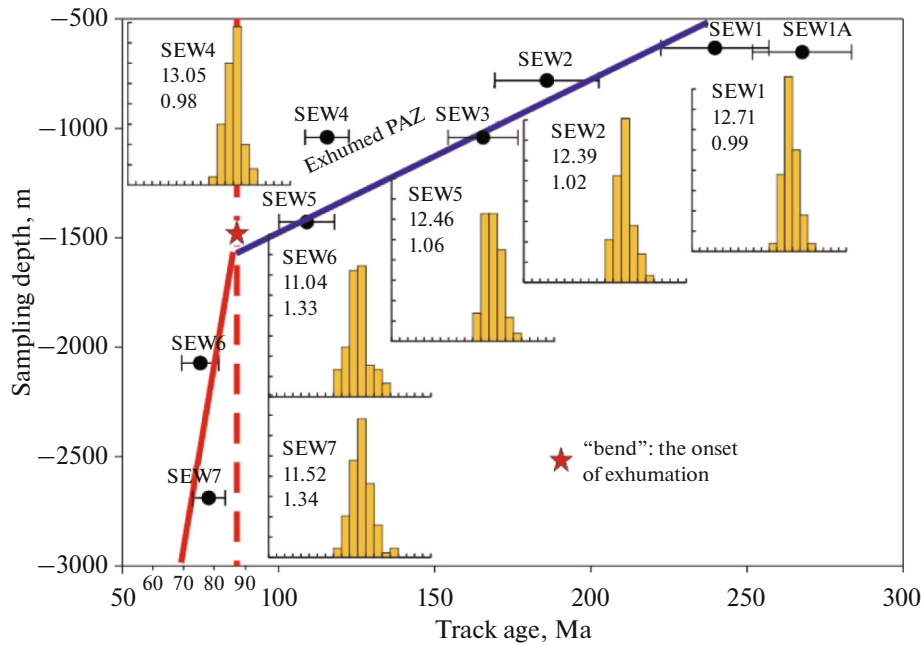


Fig. 4. Distribution of apatite track ages from Severnaya borehole on Graham Bell Island, Franz Josef Land. Graph shows classic shape of exhumed partial annealing zone (PAZ) (based on data from [85, 86, 91]); track age ($\pm 1\sigma$) is given as a function of from sampling depth; shown: representative track length distributions with sample numbers (mean length (μm) and standard deviation (μm)); lower boundary (star in red) of exhumed partial annealing zone indicates onset of rapid exhumation.

to maximum) paleotemperature in the Jurassic–Early Lower Cretaceous (Fig. 5).

The section below ~ 700 m was subjected to the influence of elevated paleotemperatures, sufficient for complete annealing of tracks in apatite, while samples located hypsometrically higher (~ 700 m) were not tested for annealing of tracks in apatite. The entire section then underwent slow cooling (exhumation) in the Early Cretaceous, accelerating in the Late Cretaceous ~ 90 Ma (Fig. 5).

Obvious evidence of Late Cretaceous (~ 95 – 88 Ma) rock exhumation over a large area of the Western Arctic, correlated in time (~ 96 – 89 Ma) with widespread

magmatism in the Sverdrup Basin of the Canadian Arctic Archipelago, on the Alpha Ridge and northern part of the Verkhoyansk fold-thrust belt near the coast of the Laptev Sea, coincides well with the time of the spread of rifting from the North Atlantic to the Arctic Basin [25, 61, 79, 80, 114, 148, 165] (Figs. 6, 7a, 7b).

RIFTING IN THE CENOMANIAN–CONIACIAN INTERVAL (~ 96 – 88 Ma)

North Atlantic Rifting Stage

In the northern segment of the North Atlantic between Greenland and Eurasia, the conjugate

Table 3. Data on track age of apatite in Severnaya borehole core obtained by combined method track and U/Pb LA-ICP-MS dating

| Sample | Quantity of grains | D_{par} , μm | D_{per} , μm | N_s , tracks | Square analysis, cm^2 | Average grain area, cm^2 | Zeta | 1σ pZeta | ^{238}U , g/t | χ^2 | Combined age, Ma | -1σ | $+1\sigma$ |
|--------|--------------------|----------------------------------|----------------------------------|----------------|--------------------------------|-----------------------------------|---------|-----------------|------------------------|----------|------------------|------------|------------|
| SEV1A | 39 | 2.03 | 0.41 | 1967 | 8.90E-05 | 4.71E-07 | 12.3570 | 0.2251 | 23.62 | 0 | 267.5 | 15.0 | 15.9 |
| SEV3 | 40 | 1.95 | 0.38 | 1465 | 1.08E-04 | 1.05E-06 | 12.3570 | 0.2251 | 12.26 | 0 | 165.3 | 10.5 | 11.2 |

Table 4. Data on length of tracks in apatite from Severnaya borehole core

| Sample | Tracks | Average length of tracks, μm | Error $\pm 1\sigma$, μd | Std _{dev} , μm | Asymmetry | Skew coefficient | D_{par} , μm | D_{per} , μm |
|--------|--------|---|-------------------------------------|------------------------------------|-----------|------------------|----------------------------------|----------------------------------|
| SEV1A | 151 | 12.77 | 0.11 | 1.30 | −0.28 | −0.77 | 1.86 | 0.33 |
| SEV3 | 152 | 13.31 | 0.09 | 1.13 | −0.22 | 0.16 | 1.86 | 0.38 |

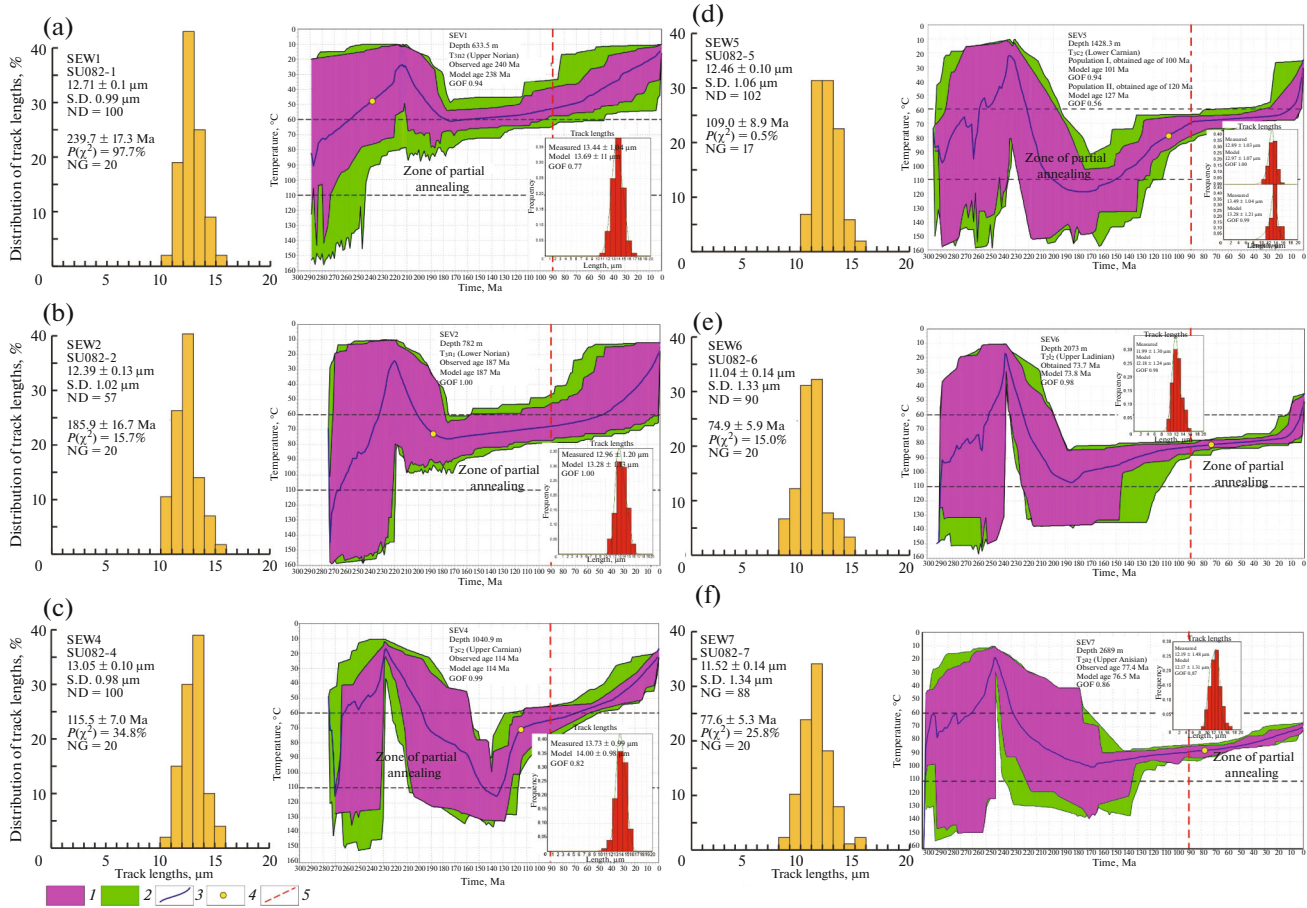


Fig. 5. Results of track analysis of apatite from samples taken from core of Severnaya borehole on Graham Bell Island, Franz Josef Land Archipelago. (a)–(f) Samples: (a), SEW1, (b), SEW2, (c), SEW4, (d), SEW5, (e), SEW6, (f), SEW7. Models were constructed using HeFTy program [117]. Notation: GOF (goodness of fit). 1–2, correspondence models: 1, good; 2, acceptable; 3, average weighted trajectory of sample; 4, combined track age; 5, onset of exhumation.

continental margins of the North Atlantic reflect a long and complex history of multiple post-Caledonian stages of continental extension accompanied by the formation of rift basins. The earliest stages of extension in the eastern segment of the North Atlantic occurred in the Middle Carboniferous, Carboniferous–Permian, and Permian–Triassic [64].

The formed rift structures of the early stages of extension were superimposed by later stages of extension that occurred in the Late Triassic–Early Jurassic, Late Jurassic–Early Cretaceous and in the Late Cretaceous–Early Paleogene [47, 82, 83].

According to plate tectonic reconstructions, the active phase of continental extension between Greenland and Eurasia began in the Late Jurassic ~200 Ma [43]. In the northern part of the Norwegian–Greenland basin, the last two stages of extension, which occurred in the Late Jurassic–Early Cretaceous and Late Cretaceous–Early Paleogene, are clearly recorded [45, 82, 83] (Figs. 6, 7a).

The beginning of the Late Cretaceous extension stage is correlated with the Cenomanian–Turonian

(~95–90 Ma) stage of rock exhumation from the northeastern coast of Greenland and Bear Island, which is located in the central part of the western margin of the Barents Sea [109, 110, 167] (Figs. 6, 7a).

In the Late Cretaceous, the Greenland and Eurasian plates between Svalbard and northeast Greenland were connected by a land bridge [156, 158]. Deformation of the continental bridge began in the Late Cretaceous ~88–80 Ma as a result of the onset of active rifting in the Labrador Sea–Baffin Bay system west of Greenland and simultaneous rifting in the Norwegian–Greenland Basin east of Greenland [69, 104, 120]. This event is clearly recorded by the beginning of rock exhumation in northwestern Svalbard (~88 Ma) and the northeastern coast of Greenland (115 (95 (?))–90 Ma) [66, 67, 109, 110] (Figs. 6, 7a).

The initial stage of lithospheric stretching between the future independent North American and Greenland plates began in the Late Jurassic (possibly in the Early Cretaceous (~140–130 Ma) [51, 123].

The Labrador Sea and Baffin Bay, formed as a result of rifting and subsequent spreading, can be clas-

sified as part of the western branch of the North Atlantic. According to plate tectonic reconstructions, the active phase of extension in the segment under consideration began in the Early Cretaceous ~120 Ma [45, 104].

Early Cretaceous rifting resulted in the deposition of detrital sedimentary rocks in half-grabens and grabens along the southwestern margin of Greenland and located opposite the Canadian margin (Figs. 6, 7a).

The northeastern Greenland part of Baffin Bay underwent intense extension and rifting during the Cretaceous–Early Paleocene, which led to the formation of a complex sediment-filled system of northwest-trending coupled grabens in Melville Bay, parallel to the coastline [100].

As a result of episodic rifting, sedimentary basins were formed, separated by ridges [100] (Figs. 6, 7a).

In the largest basin, the Melville Bay graben, the sedimentary sequence reaches >13 km [166]. In the Kiviok Basin, located west of Melville Bay, the sedimentary sequence reaches >10 km [100]. Deep seismic studies show strongly reduced thicknesses of the continental crust up to 14 km in the Melville Bay graben, which is close in value to the continent–ocean transition zone and ~18 km in the Kiviok Basin [40].

The lower sedimentary strata identified in the Kiviok Basin and Melville Bay graben have not been penetrated by drilling, so their stratigraphic reference is based on general tectonic concepts of regional development. The very bottom of the sedimentary strata could have formed in the prerift stage, starting from the Paleozoic. The sediments lying slightly higher and making up the bulk of the formation belong to the synrift stage of the Early Cretaceous–Early Cenomanian [100].

An assumption was made about the metamorphosis of sedimentary rocks of this formation and the presence of intrusions [100]. This is confirmed by deep seismic sounding results, which recorded velocities from 4.5 to 4.9 km/s at the maximum thickness of this sequence in Melville Bay graben ~7 km [40]. Roof thickness is considered a regional unconformity, probably of Mesozoic age, and is conventionally accepted as the boundary between the Upper and Lower Cretaceous or is located in the Lower Cenomanian (~98 Ma) [39, 100].

On seismic profiles, the overlying Upper Cretaceous strata, up to 6 km thick, traced in the Melville Bay graben and in the Kiviok basin, sharply thins (almost to disappearance) on the Melville and Kiviok Ridges. Dredging of rocks on the slopes of the ridges in Melville Bay reveals the significant presence of Upper Cretaceous (Cenomanian–Turonian) sediments [146]. The age of the roof of this layer is taken as Upper Cretaceous [146].

The sediments formed during the synrift stage, but during which there were periods of tectonic quietus, as a result of which seismic units with subparallel reflections formed within the strata [100].

Seismic data clearly record a tectonic event that caused a contrasting horizon separating the lower sedimentary strata (Lower Cretaceous–Lower Cenomanian) from the overlying one (Cenomanian–Cretaceous, Upper Cretaceous deposits) [100]. In the lower sedimentary layer, a classic extension-related fault system is distinguished.

The fault system can be clearly traced within the entire section of the lower sedimentary strata, associated with compression and not traceable in the overlying sedimentary strata. Narrow, elongated basins embedded in the Cretaceous and showing signs of inversion/inversions (?) are located to the northwest of the Melville Bay graben and extend to the Carey Basin [100, 102].

The relatively deep, ~5 km, south–north-oriented Carey Basin also shows evidence of intense inversion and superposition of flower-type structures [107]. North of the Carey Basin between the northwest coast of Greenland and southwest coast of Ellesmere Island is a shallow ~3 km Northern Waters Basin, oriented from northwest to southeast [140]. In this area on the coast of Ellesmere Island, exhumed rocks beginning in the Turonian ~90 Ma have been found [101].

Formation of the Sverdrup Sedimentary Basin

North of Greenland and Baffin Bay lie the Queen Elizabeth Islands of the Canadian Arctic Archipelago, within which the Sverdrup Basin is located, which is an intracratonic basin of the post-Ellesmere orogeny [155]. It extends for ~1300 km in length with a maximum width of up to 400 km and is filled with an assemblage of carbonate and detrital sedimentary rocks, starting from the Carboniferous and ending with the Paleogene, with a total thickness of up to 15 km [76]. The last stage of accumulation of coarse-grained sediments in the Sverdrup Basin occurred in the Late Cretaceous–Early Oligocene [80].

The formation of the Sverdrup Basin was completed with the nonmarine Eureka Sound Formation, locally controlled by the Late Cretaceous and Paleogene fault systems of the Eureka orogeny [141, 150]. These fault systems often represent reactivated Ellesmere and older structures [144].

The uppermost Neogene to recent sequence, the Arctic Coastal Plain, is a wedge of seaward-dipping fluvial and marine strata deposited along the modern northern passive continental margin.

Most of the Mesozoic section is intruded by Cretaceous sills and dikes of mafic, subalkaline, and alkaline composition, belonging to the High Arctic Igneous Province (HALIP) [61, 77, 79]. According to generalized geochronological results, three stages of magmatic activation have been recorded with ages of [61]:

- 122 ± 4 Ma (first stage);
- 95 ± 4 Ma (second stage);
- 81 ± 4 Ma (third stage).

The first stage affected a significant area of the Arctic, manifesting itself in Svalbard, Franz Josef Land, and the De Long Islands [58, 79, 80, 145].

The second stage of Late Cretaceous Cenomanian–Turonian magmatism with an age of 95 ± 4 Ma [61] is widely manifested in the Sverdrup Basin (Figs. 6, 7a, 7b).

On Axel Heiberg Island in clay shales and fine-grained sandstones, subaerial tholeiitic and subalkaline basalt flows are distinguished, related to the formation Strand Fjord, stratigraphically dated to the Late Albian–Early Cenomanian [76, 77]. This stage of magmatism is associated with the formation of the largest volume of igneous rocks within the Sverdrup Basin [77].

In the eastern part of Axel Heiberg Island, the thickness of the formation reaches 250 m, while its thickness in the west and north reaches 800 m. The absolute age of tholeiitic basalts of the Strand Fjord formation, obtained by the $^{40}\text{Ar}/^{39}\text{Ar}$ method (95 ± 0.2 Ma) is confirmed by U–Pb dating of baddeleyite (95.18 ± 0.35 and 95.41 ± 0.12 Ma) isolated from samples collected from a diabase dike and gabbro sill on the west coast of Axel Heiberg Island [118, 157].

According to [79], the lower age interval of the Strand Fjord formation obtained by the $^{40}\text{Ar}/^{39}\text{Ar}$ method is 100.7 Ma, but it is characterized by a significant determination error of ± 5.8 Ma, which allows us to consider this dating close to the age of 95 Ma.

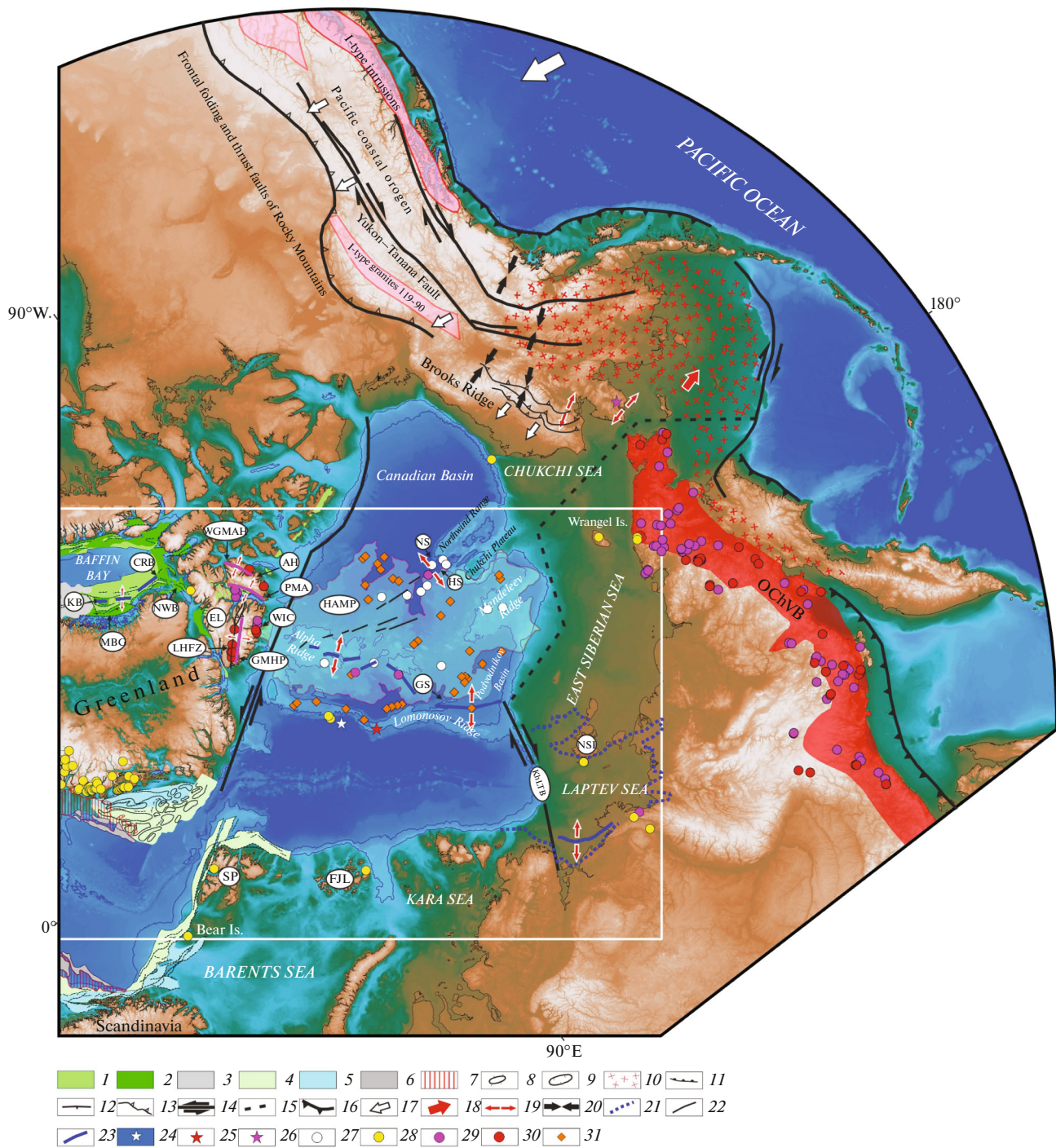
The upper age interval obtained by the $^{40}\text{Ar}/^{39}\text{Ar}$ method for a sample of tholeiitic lavas collected on the west coast of Axel Heiberg Island is 80.70 ± 1.1 Ma [163]. However, the location of the sampling sites is quite close to the sampling point of ~ 95 Ma samples obtained by the U–Pb method [118]. On the north-west coast of the Axel Heiberg Island, by $^{40}\text{Ar}/^{39}\text{Ar}$ dates of samples from nearby tholeiitic lavas are known, with ages of 80.7 ± 1.1 , 92.3 ± 1.1 , and 96.1 ± 1.9 Ma [163].

On Ellesmere Island, an analogue of the Strand Fjord Formation of Axel Heiberg Island is the Hassel Formation, which formed in the Late Albian to Early Cenomanian and consisting of nonmarine fine-grained, poorly cemented white quartz sandstones, basalts, mudrocks, and coal deposited in a deltaic setting [142].

The Hassel Formation is unconformably overlain by Upper Paleocene and Oligocene detrital deposits, up to 900 m thick, of the Eureka Sound Group [126]. For the west coast of Ellesmere Island, the age of tholeiitic intrusions obtained by the U–Pb method is 91.7 ± 1.1 and 91.7 ± 1 Ma and coincides with the determination obtained by the $^{40}\text{Ar}/^{39}\text{Ar}$ method: 91.7 ± 0.1 [59]. The age of basaltic dikes and sills collected in the fault zone of Lake Khazen and determined by the $^{40}\text{Ar}/^{39}\text{Ar}$ method fluctuates from 98.2 ± 4 to 97.9 ± 4 Ma [79].

On the northern coast of Ellesmere, the Wootton intrusive complex is known, which is a bimodal

Fig. 6. Established Late Cretaceous (Cenomanian–Coniacian) manifestations of rock exhumation with age of 95–90 (88) Ma and magmatism with age of 98–88 Ma in Arctic, on coast of North Atlantic, and on northern Pacific margin of Asia and North America. Digital relief base IBCAO v.4 (according to [111]). Rock exhumation with age of 95–90 (88) Ma (according to [4, 66, 67, 97, 101, 102, 109, 110, 119, 126, 148, 167]). Manifestation of magmatism with age of 98–92 for: Ellesmere Island and Axel Heiberg Island (according to [61, 79, 80, 118, 157, 163]) for Amerasian Basin (according to [114, 132, 164]); eastern sector of Arctic, as well as territories adjacent to Laptev Sea, and Pacific margin of Russia, Alaska, and North American Cordillera (according to [38, 127–129, 147]). Established manifestations of magmatism in Amerasian Basin are of a different age or undated (according to [22, 31, 49, 94, 108, 132, 162]). Position of igneous objects identified by seismic data (according to [22, 122, 137]); rift structures of Baffin Bay (according to [40, 98, 138]); Late Jurassic–Early Paleogene basins of northern part of Norwegian–Greenland basin (according to [82, 83, 92]); main transform faults within Arctic Basin (according to [21]); contour of Laptev Sea rift system (according to [2, 28, 29, 69, 70]); key elements of Pacific margins of Russia, Alaska, and North American Cordillera (according to [38]). Position is shown in Fig. 7 (white frame). *Barents Sea*: SV, Svalbard; FJL, Franz Josef Land archipelago; *Laptev Sea*: NI, Novosibirsk Islands; KhLTR, Khatango–Lomonosov Transform Fault; *Baffin Bay*: B, Bylot Island; MBG, Melville Bay graben; KB, Kiviok Basin; KrB, Kerry Basin; NWB, Northern Waters Basin; *Sverdrup Basin*: AH, Axel Heiberg Island; EL, Ellesmere Island, LHFZ, Lake Hazen fault zone; WIC, Wootton intrusive complex; WGMHI, western gravimetric maximum of Axel Heiberg Island; PMA, Princess Margaret Arc; HPGM, Hazen Plateau Gravimetric Maximum; *Arctic Basin*: HALIP, High Arctic Large Igneous Province according to magnetic data (according to [139]), (translucent fill in pale yellow); GS, Geofizikov spur; HS, Healy spur; NS, Northwind Ridge spur; OChVB, Okhotsk–Chukotka volcanic belt (according to [38]) (translucent red background). 1–3, Baffin Bay and adjacent land: 1, Cretaceous–Cenozoic sedimentary basins; 2, basins that began to form in Early Cretaceous; 3, main area of distribution of Paleogene magmatism in Baffin Bay; (5–11) shelf and slope areas and structures of northeastern Greenland, Scandinavia, and western Barents Sea; 4–5, rift basins: 4, Late Cretaceous–Paleocene; 5, Late Jurassic–Early Cretaceous; 6–7, areas of distribution of magmatic manifestations: 6, igneous flows of indeterminate age (Lower Paleogene (?)); 7, seismic complexes of SDRs type; (8–9) shelf and slope structures: 8, highs; 9, lows; 10, area of distribution of volcanic rocks with age of 105–60 Ma (Bering Strait and Alaska); 11–16, faults: 11, normal (Baffin Bay, shelf and slope structures of northeastern Greenland, Scandinavia, and western Barents Sea); 12, compression (Melville Bay graben, Greenland part of Baffin Bay); 13, crustal (Ellesmere Island, Brooks Ridge); 14, transform; 15, inferred continuation of transform fault; 16, inferred position of convergent boundary in period 105–60 Ma; 17–19, direction of compression and extension: 17, general direction of compression; 18, general direction of extension; 19, stretching in local structures; 20, compression in local structures; 21, contour of Laptev Sea rift system; 22, position of axes of negative free air gravity anomalies in Amerasian Basin; 23, inferred segments of extension axis in period 92–88 Ma; 24, North Pole; 25, location of ACEX borehole on Lomonosov Ridge; 26, gneiss granite with intrusion stage ~ 95 –90 Ma; 27, manifestation of mafic magmatism in Amerasian Basin (undated or with age different from ~ 98 –89 Ma); 28, rock exhumation with age of 95–90 Ma (88 Ma for northwestern Svalbard); 29–30, dated igneous rocks by age: 29, ~ 98 –93 Ma, 30, ~ 92 –89 Ma; 31, manifestation of igneous objects according to seismic data.



alkaline plutonic association including hornblende gabbros, microgranites, and quartz syenites. The complex consists of structures with a northeastern strike and is tectonically controlled by earlier formed fault zones. According to U/Pb dating of zircons, the complex was emplaced in a short time interval: 93–92 Ma [80].

In the central part of the northern coast of Ellesmere Island basalt flows and volcanic breccias are distinguished in the Hansen Point alkaline volcanic complex [79]. The lower parts of the section are represented by basaltic breccias and tuffs, while the overlying part is represented mainly by subaerial basalt flows.

In accordance with $^{40}\text{Ar}/^{39}\text{Ar}$ According to Ar data, the age of the volcanics of this formation is distributed in the range 83.0 ± 1.8 – 73.5 ± 2.4 Ma, although the dating of the basalt dyke is known with an age of 93.9 ± 1.3 Ma, which is close to the age intervals of 96.6 ± 1.6 and 94.3 ± 2.8 Ma obtained for the nearby basalt dykes in Pyrian metasediments [79, 80].

Tholeiitic and alkaline–alkaline transitional basalt flows of ~128–95 Ma, as well as younger alkaline bimodal series, which formed around 90 and 80 Ma in the northeastern Canadian Arctic, are interpreted as part of a continental rift zone that extends parallel to the axis of the Sverdrup Basin [80]. The stages of intensive rift magmatism, which also affected the Alpha–Mendeleev ridge system, are associated with opening of the Amerasian Basin (Figs. 6, 7a).

Manifestations of Magmatism on the Pacific Coast of North America

On the Pacific coast of North America, Cretaceous magmatism in the Cordillera is limited to narrow belts of the Coastal orogens and the Omineca/British Columbia orogens [130, 131]. Cretaceous magmatism in the Cordillera is synchronous with a regional stage of crustal compression caused by subduction of the oceanic Izanagi Plate [38].

Between 115 and 95 Ma, a right-lateral strike-slip fault formed in the Omineca orogen and a left-lateral strike-slip fault formed in the Coastal orogen, resulting in a transpressional igneous environment [52, 134] (Fig. 6).

According to data [38] on magmatism in the coastal orogen from southern Canada north to Alaska, there was an intrusion of type I magmas with an age of 118–90 Ma. In the eastern Omineca region of the Canadian Cordillera, S-type granites were intruded during approximately the same time period (119–90 Ma). During this time interval, the Cordillera experienced crustal shortening (Fig. 6).

Manifestations of Magmatism in the Amerasian Basin

In the Amerasian Basin, the HALIP has been established by the nature of the high-amplitude magnetic field, contrasting reflections in the seismic record, geological sampling, and direct observations using special underwater vehicles [22, 23, 34, 49, 54, 81, 108, 114, 122, 132, 139, 154] (Figs. 6, 7a).

The first samples of alkaline basalts were dredged on the Alpha Ridge during the 1983 CESAR expedition (Canada) during ice surveys under the Polar Continental Shelf program [108, 162]. In the central part of the ridge, the $^{40}\text{Ar}/^{39}\text{Ar}$ method yielded the age of basalt as 89 ± 1 Ma [114], which coincides with isotopic age determinations (90.40 ± 0.26 Ma) of lapilli tuffs [165].

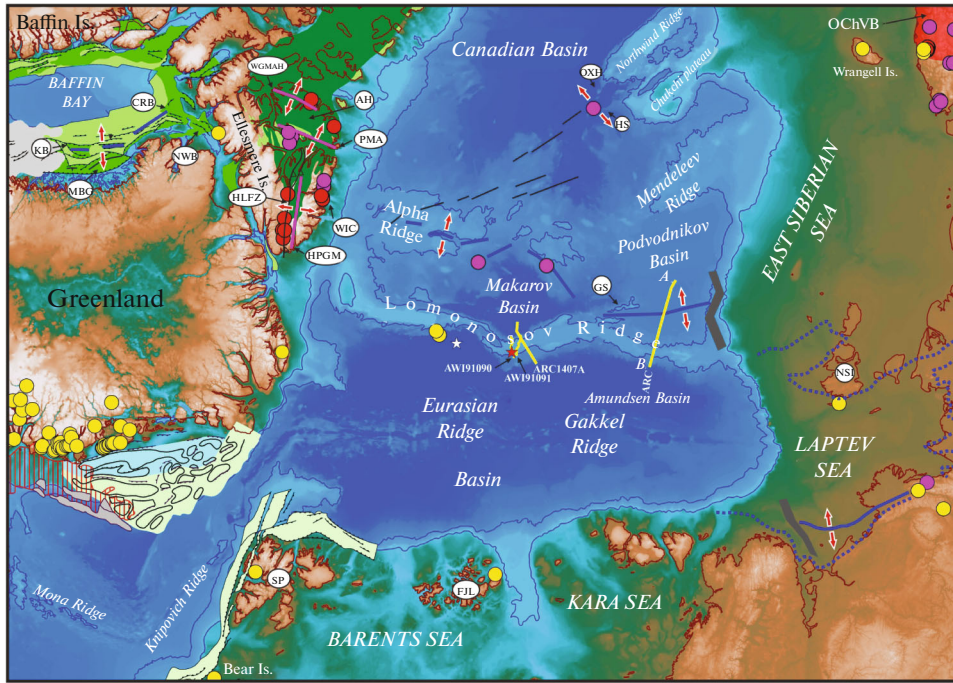
On the traverse of the Wootton intrusive complex is the central part of the Alpha Ridge, which is clearly mapped by a well-known system of local grabens, manifested in the bottom relief and gravimetric anomalies (Figs. 7a, 7b).

It can be suggested that this segmented local system formed ~95–90 Ma and is a northern continuation of the Baffin Bay–Axel Heiberg and Ellesmere Islands rift system.

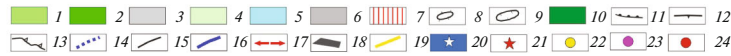
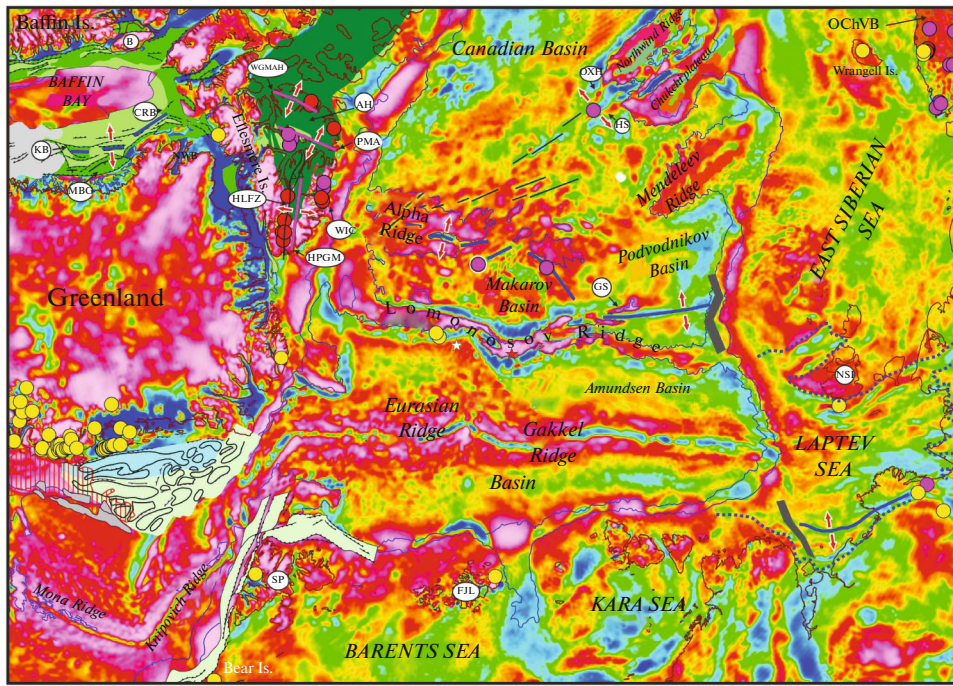
Direct observations of the slopes of the Mendeleev Ridge with the help of a research submarine (Navy Ministry of Defense, Russia) and the results of surface drilling showed that they are penetrated by intrusions

Fig. 7. Established Late Cretaceous (Cenomanian–Coniacian) manifestations of rock exhumation with age of 95–90 (88) Ma and magmatism with age of 98–88 Ma in Arctic. (a) Relief IBCAO v.4 (by [111]), (b) free air gravitational anomalies of WGM project (according to [46]). *Barents Sea:* SV, Svalbard; FJL, Franz Josef Land; *Laptev Sea:* NSI, New Siberian Islands; *Baffin Bay:* B, Bylot Island, MBG, Melville Bay graben, KB, Kiviok basin; KrB, Kerry Basin; NWB, Northern Waters Basin; *Sverdrup Basin:* AH, Axel Heiberg Island; EL, Ellesmere Island, LHFZ, Lake Hazen fault zone; WIC, Wootton intrusive complex; WGM/AHI, western gravimetric maximum of Axel Heiberg Island; PMA, Princess Margaret Arc; HPGM, Hazen Plateau Gravimetric Maximum; *Arctic Basin:* Gs, Geophysicist spur, OH, Healy spur, ON, Northwind Ridge spur; OChVB, Okhotsk–Chukotka volcanic belt (translucent red background), according to [38]. 1–3, Baffin Bay and adjacent land: 1, Cretaceous–Cenozoic sedimentary basins; 2, basins that began to form in Early Cretaceous; 3, main area of distribution of Paleogene magmatism in Baffin Bay; (5–11) *shelf and slope areas and structures of northeastern Greenland, Scandinavia, and western Barents Sea;* 4–5, rift basins: 4, Late Cretaceous–Paleocene; 5, Late Jurassic–Early Cretaceous; 6–7, areas of distribution of magmatic manifestations: 6, igneous flows of indeterminate age (Lower Paleogene (?)); 7, seismic complexes of SDRs type; 8–9, shelf and slope structures: 8, highs, 9, lows; 10, Sverdrup Basin (Carboniferous–Cretaceous); 11–13, faults: 11, normal (Baffin Bay, shelf and slope structures of northeastern Greenland, Scandinavia and western Barents Sea); 12, compression (Melville Bay graben, Greenland part of Baffin Bay); 13, crustal (Ellesmere Island); 14, contour of Laptev Sea rift system; 15, position of axes of negative free air gravity anomalies in Amerasian Basin; 16, inferred segments of extension axis in period 92–88 Ma; 17, direction of stretching; 18, Upper Cretaceous system of local pull-apart basins; 19, position of seismic profiles (AWI91090 and AWI91091 according to [116]), ARC according to [23]); 20, North Pole; 21, position of ACEX borehole on Lomonosov Ridge; 22, rock exhumation with age of 95–90 Ma (88 Ma for northwestern Svalbard); 23–24, dated igneous rocks by age: 23, ~98–93 Ma; 24, ~92–89 Ma.

(a)



(b)



of the type of dikes and sills of Barremian–Albian age [31, 154]. At the same time, the peak of Lower Cretaceous magmatism is concentrated in the narrow range of 110–114 Ma [154].

In igneous rock samples, single zircon grains with an isotopic age of 83–87 Ma were found, the formation of which is associated with crystallization of Lower Cretaceous zircons as a result of the influence of the stage of Upper Cretaceous magmatism, manifested within the HALIP.

Between Alaska and the Lomonosov Ridge is a stark, recognizable structure in any remote sensing data, uniting the Chukchi Plateau and the Northwind Ridge [132] (Figs. 6, 7a, 7b).

Isotopic dating by $^{40}\text{Ar}/^{39}\text{Ar}$ analysis of low- and high-titanium tholeiitic basalts dredged on submarine slopes just north of the Chukchi Plateau and Northwind Ridge showed their Cretaceous age (118–112, 105–100, and 90–70 Ma) [49, 94, 132].

For the Healy spur, which is the northern continuation of the Chukchi Plateau, there are two dates: 88.98 ± 1.37 and 90.27 ± 1.15 Ma [132] (Figs. 6, 7a, 7b).

The northern region, located between the Northwind Ridge and the Chukchi Plateau and their continuations into the Amerasian Basin in the form of the Northwind and Healy spurs, has clear traces of stretching [54], which is clearly visible in the bottom relief and gravity anomalies in the northern direction towards the Alpha Ridge (Figs. 6, 7a, 7b).

In the section of the sedimentary cover on the Alaskan shelf, the surface of an unconformity with an age of ~90 Ma is distinguished [95, 102]. The attribution of this age to the boundary is partly based on the results of thermogeochronological studies of sedimentary rock samples taken from the northernmost Popcorn borehole (Fig. 7a).

According to the estimates obtained, rock exhumation is recorded in the interval of ~90–65 Ma [97]. On the Pacific coast of Eurasia ~106–76 Ma, the continental margin Okhotsk–Chukotka volcanoplutonic belt was formed [38]. The most intense volcanic activity occurred ~90–84 Ma [38].

A comprehensive geological study was carried out, including thermogeochronological studies, for Wrangel Island and coastal Chukotka located to the south of it. The formation of plutons in Chukotka occurred 108–100 Ma, followed by rapid cooling ~95 Ma (biotite, $^{40}\text{Ar}/^{39}\text{Ar}$) [127]. Uplift, erosion, and development of a regional unconformity ~89 Ma are associated with a weakening of magmatism in the area as it moved south to form the Okhotsk–Chukotka volcanic belt in a neutral to weak extensional tectonic setting [127].

Analysis of Seismic Data for the Central and Eastern Parts of the Lomonosov Ridge

As numerous geological and geophysical studies have established, the Lomonosov Ridge is a block of

continental crust that before the opening of the Eurasian Basin, which began in the Early Paleogene, was located along the northern edge of the modern shelf of the Barents and Kara seas [8, 23, 26, 41, 48, 112, 115, 116, 119].

Starting from the ACEX boreholes, located approximately in the center of the Lomonosov Ridge, to the lateral continental margin of the East Siberian Sea, the Lomonosov Ridge is quite well studied in the seismic aspect [115, 121, 137] (Figs. 6, 7a).

The ACEX deepsea drilling project, located along seismic profile line AWI91090 on the Lomonosov Ridge, having passed 404.8 m to the level of Cenozoic deposits, has exposed rocks lying below the surface of the regional unconformity identified on seismic profiles [115] (Figs. 7a, 8).

The rocks are represented by compacted sands, sandstones, and argillites hosting agglutinated foraminifera, dinoflagellates, as well as spores and pollen [44]. Dinoflagellates isolated from deposits of this part of the section were identified as pre-Maastrichtian and Campanian [43]. A hiatus in sedimentation lasting >15 Ma was established above the Upper Cretaceous rocks, since the overlying black clays, based on dinoflagellates, were identified as Late Paleocene and their formation is associated with the onset of spreading in the Eurasian Basin [43, 44].

The study of spore–pollen complexes from rock samples in the lowest part of the borehole determines the Upper Cretaceous (Maastrichtian)–Paleocene (Danish) age, although it is noted that this interval has a wider stratigraphic interval: Campanian–Maastrichtian, possibly Campanian–Danian [10].

When referencing the position of the ACEX borehole to seismic profile AWI91090, in the lowest part, the borehole section falls into the upper part of the half-graben, towards the Eurasian Basin; i.e., a Campanian age of the lowest deposits located in the half-graben can be accepted [116] (Fig. 9a).

On the close profile AWI91091, the part of the ridge directed towards the Eurasian Basin is characterized by truncated filling in half-grabens, and on the opposite side, the progradation of the underlying sediments towards the Makarov Basin is clearly visible [115, 121] (Fig. 9b).

A similar pattern is observed for seismic profile ARC1407A (Fig. 9c).

Discovered in the northeast of Franz Josef Land, the onset of rock exhumation ~90 Ma correlates with the age of the onset of cooling of rocks (~95 Ma) collected on the modern slope of the Lomonosov Ridge from the Amundsen Basin and opposite the western part of Franz Josef Land [119] (Figs. 6, 7a).

This caused the progradation of sediments from the Barents–Kara margin (its composition included the Lomonosov Ridge) towards the Amerasian Basin, which led to the formation of sediments on the slope

of the Lomonosov Ridge from the Makarov Basin. In this case, the lowermost part of the sedimentary cover, located above the surface of the acoustic basement, presumably began to form in the Cenomanian–Turonian (~95–90 Ma).

RESULTS

The presented data partly coincide with the fact that the slope of the Lomonosov Ridge towards the Eurasian Basin is characterized by Paleocene rifts that preceded the opening of the Eurasian Basin, while the opposite slope is characterized by Cretaceous rifts [23]. Although there is a difference in the interpretation of the age of the sediments, in [23], the age of the Cretaceous rifts and, consequently, the lower part of the sedimentary strata is taken as Aptian–Albian (older than 100 Ma), synchronous with the age of the rifts of the Podvodnikov Basin.

In [23], the ARC composite seismic profile was published, a fragment of which begins in the Amundsen Basin and crosses the Lomonosov Ridge, Lomonosov terrace, and Geofizikov spur and ends in the Podvodnikov Basin (Fig. 8). According to the nature of the bottom relief, the area between the Lomonosov Ridge and the Geofizikov section is called the Lomonosov terrace [23]. Based on the nature of the relief of the surface of the acoustic basement, the area belongs to a local rift basin [23], which we have conditionally called the Geofizikov Basin.

In the center of the basin is a local uplift with characteristic contrasting reflections, suggesting its igneous nature (volcano (?)). The rift basin is clearly visible in gravity anomalies as a linear minimum, which continues to the edge of the continental slope of the East Siberian Sea (Fig. 7b). We suggest that the Geofizikov rift basin began to form in the Cenomanian–Turonian (~95–90 Ma) and connected with the northern end of the rift system of the Alpha Ridge Fracture Zone.

In the south, the Geofizikov rift basin abuts the inferred Khatanga–Lomonosov transform fault, identified in some studies [14, 21, 65, 70, 95], along which the Lomonosov Ridge moved with respect to the continental margin during the Cenozoic due to opening of the Eurasian Basin. There is no consensus on either the existence or formation age of this hypothetical transform fault.

Based on Russian seismic data, the deep Vilkitsky trough with a sedimentary sequence of up to 5.5 km has been identified, separating the Lomonosov Ridge from the De Long Massif, in the northwestern East Siberian Sea [26]. The idea of the continuity of the supporting reflectors extending from the shelf side through the Vilkitsky trough and continuing onto the Lomonosov Ridge has been confirmed, although this is applicable only to the upper part of the sedimentary section. In the seismic record, vertical faults in the

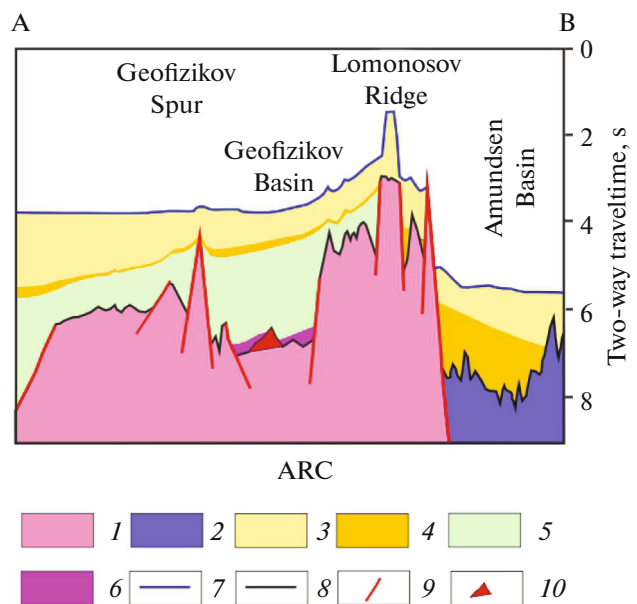


Fig. 8. Fragment composite seismic profile ARC (according to [23], modified). 1–2, Type of crust: 1, continental reduced; 2, oceanic; 3–5, sedimentary cover: 3, Upper Cenozoic; 4, Lower Cenozoic; 5, Cretaceous (<90 Ma (?)); 6, contrasting reflections in lower part of deposits, igneous objects (?); 7, bottom topography; 8, basement relief; 9, faults; 10, volcano (?).

middle and lower parts of the sedimentary cover section in the basin are identified with normal faults, not transform faults, so the existence of the Khatanga–Lomonosov transform fault is disputed [26].

In [135], the possibility of transform movement of the Lomonosov Ridge along the eastern part of the continental margin of the Laptev Sea is allowed only during the period of the initial spreading history of the Eurasian Basin. According to the geodynamic model [21], the existence of a transform fault is substantiated from the onset of spreading in the Eurasian Basin (~57 Ma) until its slowdown (~44 Ma), associated with cessation of the Pacific Kula Plate.

Based on the interpretation of a larger amount of seismic data, it is suggested that local depressions in the sedimentary cover located above faults in the basement of the Vilkitsky trough may be traces of the Khatanga–Lomonosov transform fault, which existed without significant horizontal offsets [136]. The seismic profile crossing the southeastern Eurasian Basin, the Lomonosov Ridge and the adjacent Podvodnikov Basin records the absence of disturbances in the Cenozoic sediments, which allows us to suggest possible transform movement along the Khatanga–Lomonosov fault only during the prespreading history of the Eurasian Basin [113, 114] (Figs. 7a, 7b).

In [23] it is suggested that in the south, the continuation of the Geofizikov rift basin is the East Anisinsky Basin, located parallel to the edge of the continental

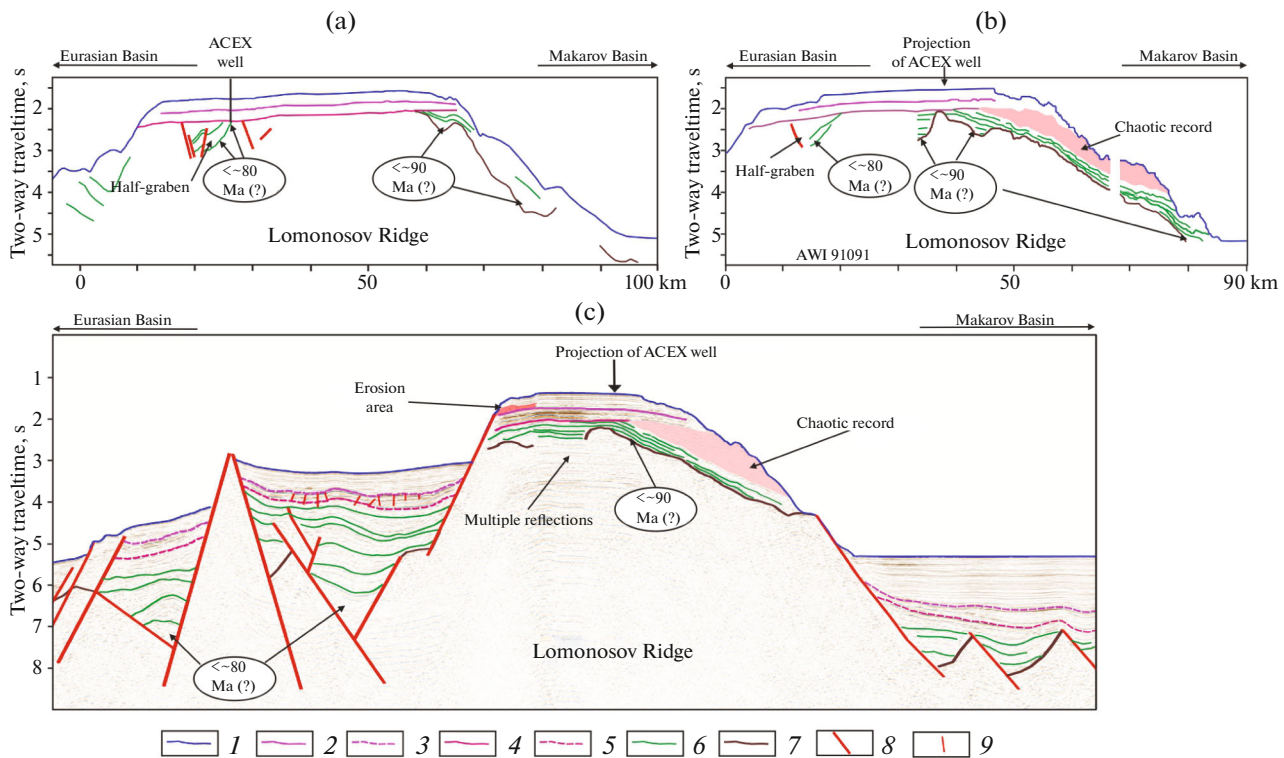


Fig. 9. Interpretation of seismic profiles AWI91090, AWI91091 and ARC1407A (fragment). For position of profiles, see Fig. 7a. (a)–(c), Seismic profiles: (a) AWI91090 (according to [112, 116]); (b) AWI91091 (according to [112, 116]); (c) ARC1407A (fragment) (according to [135]). 1–7, Geological boundaries: 1, bottom; 2, unconformity boundary (44.4–18.2 Ma); 3, inferred position of unconformity boundary (44.4–18.2 Ma); 4, unconformity boundary corresponding to onset of spreading in Eurasian Basin (57.4 Ma); 5, inferred position of unconformity boundary corresponding to onset of spreading in Eurasian Basin (57.4 Ma); 6, characteristic reflections in sedimentary cover of Upper Cretaceous (?) age; 7, acoustic basement; 7–8, faults: 8, major; 9, in Paleogene (57.4–44.4 Ma) sedimentary cover.

shelf, but the question of the further continuation of the opening axis within the Laptev Sea remains open.

The structure of the Laptev Sea shelf is represented by a series of deep rifts and high-standing basement blocks, forming a complex rift system. Two main systems are distinguished [28, 29]:

- the western system, which includes the South Laptev rift basin and the Ust’–Lena rift;
- the eastern system, which includes the East Laptev horst and graben province, and the Belkovsko–Svyatonosky, Anisinsky, and Novosibirsk rifts.

The formation of the rift system is connected with the fact that this region during the last 70–60 Ma was one of the segments of the boundary of the North American and Eurasian plates in the Arctic [11, 70]. Seismic data reliably record a decrease in the thickness of sediments in rift basins from west to east, which suggests a rejuvenation of rifting to the east in the Upper Cretaceous [12].

A series of plate tectonic reconstructions allows for the reverse direction of rift migration from east to west [136], although seismic data convincingly indicate an almost twofold increase in the depth of the western basins (the South Laptev rift basin and the Ust’–Lena

rift), compared to the eastern basins (the Belkovsko–Svyatonosky, Anisinsky, and Novosibirsk rifts) [69, 70].

We hew to the hypothesis of eastward migration of the system [12].

The western contour of the Laptev Sea rift system, presented in [70], differs slightly from the results of generalizations carried out during compilation of the State Geological Map of the Russian Federation at a scale of 1 : 1 000 000 [2, 28, 29]. The South Laptev rift basin (western system of the Laptev Sea) continues to the northwestern part of the Lena Delta region [28, 29]. The boundary of the rift system within the Lena River delta stands out in controversy.

In [70], in this segment the border is drawn near the shoreline of the Lena River.

In [2], almost the entire Lena River delta is considered to be affected by Cretaceous–Cenozoic rifting. On the southern continuation of the South Laptev rift basin in the northwestern part of the Verkhoysk fold–thrust system are the superimposed Kengdei, Soginsky, Kunginsky, Khara–Ulakhsky, and Khorogorsky grabens, as well as the western part of the Bykovsky graben, located on land [5]. All of them consist of Paleogene continental deposits. The largest, Kengdei

graben is about 90 km long and up to 8–12 km wide and extends NNE.

Study [70] shows the correlation of the rift and graben system of the Laptev Sea with the regional anomalous gravitational field and, if we orient ourselves towards this, the largest linear grabens are clearly located inside the elongated negative anomaly, which can be traced along the continuation of the South Laptev rift system (Fig. 7b).

Near the Soginsky, Kengdeysky, and Kunginsky grabens, thin, usually linear dikes are distinguished, belonging to the Soginsky Complex, the emplacement of which is associated with graben formation [5]. The trachybasalt and subalkaline dolerite dikes are 2–50 m thick, 2–7 km long, and lie vertically among Carboniferous–Permian terrigenous deposits, although the length of one of the dikes reaches 18 km. The age of two dikes determined by U/Pb by method is 86 ± 4 and 89 ± 2 Ma, which is associated with the initial rifting that preceded opening of the Eurasian Basin [148].

Supporting this viewpoint, we suggest that ~95–90 Ma, continental rifting began in the western–South Laptev–rift system, which migrated further from east to west [12]. In this case, the connection of the Geofizikov rift basin with the South Laptev basin could have occurred along a local transform fault that existed only during the prespreading history of the Eurasian Basin, as suggested earlier in [114]. We believe that in the initial stage of rifting in the Upper Cretaceous, there was no single transform fault, and the connection occurred through a system of local pull-apart basins.

During the Cenozoic spreading history of the Eurasian Basin in the Paleogene, changes in the direction of basin opening occurred [88], which could have caused short-term reactivation of individual segments of the system of local pull-apart basins and ultimately the formation of the East Anisinsky Basin. In this case, the lowest layers of the sedimentary cover, distinguished in the northern part of the South Laptev rift system and in the East Anisinsky Basin, may be represented by Cenomanian–Turonian continental deposits.

RECONSTRUCTION OF THE POSITION OF THE RIFT STRUCTURE

The geodynamic evolution of the eastern sector of the Arctic in the Cretaceous and Cenozoic is largely associated with subduction of the oceanic lithosphere of the Pacific Ocean under the northeastern margin of Asia [19, 20, 32, 38, 128].

The geodynamic model of upper mantle convection beneath the lithosphere of the Arctic and Northeast Asia quite accurately explains the emergence of the Eurasian Basin as a result of movement of the Barents–Kara segment of the Eurasian Plate towards the Kula Plate, which was subducted beneath the margin of Asia [19, 20]. The Kula Plate formed from parts of

the Pacific, Izanagi, and Farallon plates ~83 Ma and became part of the Pacific Plate ~40 Ma or was completely subducted ~44 Ma [21, 160].

According to geodynamic models, displacement of the Lomonosov Ridge, which is a block of continental crust, with respect to the Eurasian margin along the Khatanga–Lomonosov transform zone, occurred from the Upper Paleocene to the Middle Eocene and is explained by the very rapid subduction (12 cm/year) of the Kula Plate under the Arctic [21]. In this case, the vectors of movement of the Kula Plate were directed orthogonally to the subduction zone [21] (Fig. 6).

According to the reconstruction for the age of the onset of the opening of the Eurasian Basin [21] in the Lower Paleogene (~57 Ma), it is suggested that there are two limiting transform zones extending towards the Pacific Ocean and limiting the Amerasian microplate, which includes the Amerasian Basin, the Chukchi Plateau, and the Northwind Ridge, a significant part of the Chukchi Sea and the Lomonosov Ridge (Fig. 6).

The first transform zone, starting from the Khatanga–Lomonosov transform fault, continues along the edge of the continental slopes of the East Siberian and northwestern part of the Chukchi Sea; along 170° E, it extends towards the Pacific Ocean. The second transform zone was presumably located along the modern foothills of northern Greenland and the Canadian Arctic Archipelago. South of the beginning of this transform zone in the Early Paleogene between the North American and Eurasian plates, the Greenland Plate formed, which existed until the Early Oligocene [51, 88, 138, 151].

In the north, the North Atlantic is divided into two parts:

- the western part, located between North America and Greenland; in the south it begins in the Labrador Sea, where spreading began ~62.5 Ma, and continues north into Baffin Bay, where spreading began ~59 Ma [45, 103, 138];

- the eastern part is located between Eurasia and Greenland, where spreading, according to the identification of linear magnetic anomalies, began ~57 Ma [87, 92].

Then, at the beginning of the Paleogene, the Arctic sector, in accordance with the reconstruction presented in [21], can be conditionally divided into three segments on a global scale.

- The Western segment, including part of North America (except for Alaska) and Greenland. On the Pacific coast of the western segment, as a result of subduction of the oceanic plate, the North American Cordillera have already formed, and between the east coast and Greenland, the Labrador Sea–Baffin Bay rift basins formed.

- The Central segment, which begins on the Pacific coast of Alaska and continues into the Amerasian Basin, including the future Lomonosov Ridge.

— The eastern segment, including northeastern Eurasia, on the Pacific coast of which, as a result of subduction of the oceanic plate, the Okhotsk–Chukotka volcanic belt was formed, and within the Arctic Basin, the rift system of the Laptev Sea had already arisen.

This assumption is based on significant differences in the geological structure and formation time of igneous belts of the Pacific margins of Russia and Alaska and the North American Cordillera [38, 128].

DISCUSSION

In [38], significant differences in magmatism along the Eurasian margin of Russia and the Pacific coast of North America were noted, associated with different tectonic settings and differences in subduction settings.

During ~119–90 Ma, shortening of the crust in the Pacific region of North America coincided with the first rifting stage in the western North Atlantic. The movement of the North American Cordillera “towards the trench” [38], which began ~125 Ma, led to “liberation” of space between North American Plate and Greenland and the onset of active rifting. Therefore, in addition to the stretching region formed by this time in the eastern North Atlantic between Greenland and Eurasia, an additional stretching region appeared. The extension axis in Baffin Bay could have been located within the grabens of Melville Bay (Figs. 7a, 7b).

Reorganization of movement of lithospheric plates that occurred ~95–88 Ma led to the beginning of deformation of the continental bridge that existed between the northeastern part of Greenland and Svalbard and the appearance of compression faults in the Lower Cretaceous–Lower Cenomanian sedimentary strata in the grabens of Melville Bay [69, 100, 104, 120].

The coincidence of the stage of magmatism and rock exhumation in the north of the North Atlantic segment ~97–90 Ma clearly indicates a sharp change in the geodynamic regime in the Pacific sector, which is confirmed by the end of the stage of granitoid magmatism in the North American Cordillera ~90 Ma [38].

Reconstruction of the history of the Pacific Ocean and its predecessor, the hypothetical Panthalassa Ocean, is largely associated with the subduction of more than 95% of the Pacific–Panthalassa lithosphere, which began in the Late Jurassic ~150 Ma [160]. The formation of oceanic crust in the Cretaceous within the Pacific–Panthalassa domain is classically modeled as a system of four major lithospheric plates: the Pacific and the surrounding Izanagi, Farallon, and Phoenix, which are thought to have existed throughout most of the Mesozoic [125, 133, 152, 153, 160].

However, the oceanic lithosphere of the Izanagi, Farallon, and Phoenix plates has been almost completely lost as a result of subduction, so the outline of their boundaries is largely determined by kinematic models associated with the absolute motion of the Pacific Plate [125, 153, 160].

The most accurate determination of the movement kinematics of the Pacific Plate is facilitated by the presence within its boundaries of a large number of hot spots: volcanic seamounts and large volcanic regions of Cretaceous age, known as large igneous provinces, which include the Shatsky, Hess, and Magellan rises; the Ontong–Java, Manihiki, and Hikurangi plateaus; the Nauru Basin, and the Mid-Pacific Mountains [50, 56, 75, 78].

A significant reorientation of hotspot traces $\sim 95 \pm 8$ Ma in the Pacific Ocean confirms the global nature and synchronicity of the plate reorganization event that occurred ~95 Ma [125, 164]. The most recent kinematic model shows that at this time, there was a sharp change in the direction of movement of the Pacific Plate, which began to move northwest with respect to the mantle plumes [160]. Such a change in the direction of movement of the Pacific Plate should have been reflected in the nearby plates: the Izanagi, which subducted under Eurasia, and the Farallon, which subducted under North America.

It is likely that the abrupt restructuring of plate movement in the northern sector of the Pacific Ocean led to tectonic restructuring in the North Atlantic segment as well. At the initial stage, reactivation of old fault sutures could have occurred, which may be evidenced by the stage of magmatism on the Ellesmere with an age of ~96–90 Ma [61, 79, 80, 118, 157].

The age of basaltic dikes and sills collected in the Lake Hazen fault zone, located in the northern part of Ellesmere Island, which is part of the Queen Elizabeth Islands of the Canadian Arctic Archipelago, determined by $^{40}\text{Ar}/^{39}\text{Ar}$ fluctuates in the range of 96.4 ± 1.6 Ma [79]. This fault zone, located along the central part of Ellesmere Island, is nearly orthogonal to the Alpha Ridge, separating the North Ellesmere domain from the more southerly stable Hazen block [140] (Figs. 6, 7a).

The Hazen block is characterized by horizontal Paleogene deposits of the Eureka Sound Group overlying steeply dipping strata of the Paleozoic Hazen fold belt, suggesting only a minor influence of Eureka deformations [53, 140]. In the gravity Bouguer anomalies, the zone separating the domain of the northern part of Ellesmere Island from the stable Hazen block is expressed by the linear gravity maximum of the Hazen Plateau [140].

Gravity modeling has shown that the depth to the Moho surface beneath most of the domain of northern Ellesmere Island and the Hazen Plateau are ~38 km apart, with the zone sharply decreasing to 32–34 km [140]. The formation history of the Ellesmere Island orogeny is highly complex and has been influenced by numerous tectonic events, culminating in the Late Devonian–Early Carboniferous Ellesmere orogeny [161].

We can assume that the initial stage of the abrupt restructuring of the direction of plate movement in the

Pacific–Panthalassa sector reactivated the old fault system of the Ellesmere orogeny, as a result of which, in the zone of detachment of the northern Ellesmere Island domain from the stable Hazen block, continental rifting occurred, accompanied by a brief pulse of basaltic magmatism.

On the west coast of Axel Heiberg Island, the U–Pb age of the basalts is ~95 Ma [118]. The position of the sampling points for basalts coincides with the axis of the linear local maximum of gravity Bouguer anomalies: the western maximum of Axel Heiberg Island [140] (Figs. 6, 7a).

West of the axis, in the middle of the Ellef–Ringnes Island, passes the Cornwall arc (arch); from the east, along the east coast of Axel Heiberg Island, the Princess Margaret arch is located [140]. Gravity modeling shows a shallow Moho surface beneath the axis and arcs (arches) at a depth of ~32–34 km [140].

This parallel south–north system, along which Cretaceous magmatism with an age of 95–81 Ma is expressed, is obviously associated with continuation of rifting from Baffin Bay [61, 80, 118, 157]. At the same time, in the north, the system is orthogonally bounded by the northern gravity maximum of the Sverdrup Basin, beneath which, according to gravity modeling, the Moho surface lies at depths of <30 km, which is ~3–6 km less than beneath adjacent crustal blocks (Figs. 6, 7a).

In general plan view, the direction of the northern gravity maximum of the Sverdrup Basin, parallel to the slope of the Amerasian Basin, coincides with the zone of detachment of the Northern Ellesmere domain from the stable Hazen block, which is also characterized by a decrease in the depth of the Moho surface.

We suggest the following scenario for the development of this segment. A study of hot spot traces, which appear on the surface of the Pacific Ocean Plate as volcanic seamounts, large volcanic regions, and submarine ridges, shows a rapid change in the direction of plate movement that occurred ~95 Ma [160].

The initial stage of an abrupt change in the direction of movement of oceanic Izanagi and Farallon plates in the Early Cenomanian resulted in compression of the Lower Cretaceous rift basins of Baffin Bay, as evidenced by compression faults in the Melville Bay graben. On Ellesmere Island, the Lake Hazen fault zone was reactivated, in which limited right-lateral movement is assumed, which predetermined the appearance of magmatism in this zone with an age of ~97–94 Ma [80].

The reorganization of the direction of plate movements in the Pacific Ocean ended quickly, so the compression stage in Baffin Bay was replaced by an extension stage directed orthogonally to the west coast of Greenland and east coast of North America. In the Sverdrup Basin, extension apparently occurred in local segments, recorded by arcuate segments of thinning of the continental crust and uplift of the Moho

surface. There is a tendency for the system to prograde to the east.

The age of basalts in the area of the western linear local maximum of gravimetric anomalies is ~95 Ma (Axel Heiberg Island) [118]; 92 Ma (near the Princess Margaret Range to Axel Heiberg Island [61].

This corresponds to the age of appearance of the Wootton intrusive complex 93–92 Ma on the northern coast of Ellesmere Island, which is structurally trending northeast and tectonically controlled by earlier formed fault zones [80].

The reorganization of the directions of movement of the Pacific Ocean plates, including their deep subducted components, ended ~90 Ma, as evidenced by completion of this stage of magmatism in the Sverdrup Basin. The extension axis in Baffin Bay ran segmentally within the Kiviok Basin and Jones Sound and continued on the east coast of the Axel Heiberg Island within the Princess Margaret arch and further was located with an offset in the region of the Wootton intrusive complex.

We believe that within the Amerasian Basin ~95–90 Ma, extension influenced the central part of the Alpha Ridge and formed a system of clearly mapped axial local grabens (Figs. 6, 7a, 7b).

Further, the extension axis continued into the Podvodnikov Basin between the Lomonosov Ridge and Geofizikov spur and connected with the southwestern grabens of the Laptev Sea rift system and influenced the adjacent northern part of the Verkhoyansk fold–thrust belt (Figs. 6, 7a, 7b).

Within the time of ~106–60 Ma, certain patterns in the general directions of compression and extension in the Pacific sector are observed [38, 127] (Fig. 6). The compression zone of the North American Cordillera continued into Alaska and affected a significant area of it. Extension is assumed only near the coast of the Chukchi Sea in the Brooks Range and in the Kigluayk granite–gneiss dome located relatively close to it in the Cretaceous, where a stage of magmatism/metamorphism with an age of ~91 Ma was recorded [42, 128].

The shelf zone of the Bering Sea is considered to have formed under conditions of general movement towards the Pacific Ocean. The most intense volcanic activity in the continental margin Okhotsk–Chukotka volcanoplutonic belt occurred ~90–84 Ma [38].

The peak of maximum volcanic activity in the period of 90–84 Ma was preceded by a decrease in magmatic activity at the end of the Cenomanian (96–94 Ma) and the beginning of the Turonian (94–92 Ma), which reflects a period of reorganization of the plate system in the Pacific Ocean as a result of a change in direction of movement of the Izanagi Plate [38].

In the Amerasian Basin, on the traverse of the Kigluayk dome (in the current position of the continents), a zone of extension was mapped between the Northwind and Healy spurs, where a stage of magma-

tism with an age of ~89–90 Ma was recorded [54, 132]. The direction of extension in this area is orthogonal to the direction of extension in Alaska (Fig. 6).

In this case, in the anomalous gravity field, a zone of extension between the Northwind and Healy spurs is mapped by a linear negative anomaly, the chains of which continue towards the southern part of the Alpha Ridge (Fig. 7b).

It is possible that two extensional zones existed in the Amerasian Basin during the Cenomanian–Turonian. In addition to the principal axis of extension, there was a secondary system that began from the southern part of the Alpha Ridge and continued in direction of extension between the Northwind and Healy spurs. The emergence of the secondary system could have been associated with different subduction regimes in the Pacific sector, manifested in as compression of North American Cordillera adjacent to Alaska and stretching to the shelf of the Bering Sea.

It can be suggested with significant degree conditionality that within the Bering Sea shelf at the beginning of the Late Cretaceous there was a boundary between two subducting oceanic plates: the Izanagi (subducting under Eurasia) and the Farallon (subducting under North America and most of Alaska).

During periods of reorganization of the directions of plate movement, one of which is the Cenomanian–Turonian stage, the boundary between the two plates, as well as their deep subducted parts, which continued into the Amerasian Basin, were corrected with respect to each other.

It is possible that the extension in the Bering Sea part of Alaska and the inferred secondary zone of extension in the Amerasian Basin are deep subducted components of the plates and return upper mantle currents. It is difficult to imagine that during the Cretaceous there was a single, continuous boundary between the two subducting plates.

We suggest the existence of a region within which, in some areas, extension occurred, while in other areas, transform movements occurred, compensating for differences in the subduction rates of plates and changes in the directions of their movements.

In the Upper Cretaceous, rifting in the Laptev Sea occurred impulsively and was subjected to restructuring of the direction of plate movements in the Pacific sector. A brief stage of activation during the period ~96–89 Ma in the Laptev Sea was replaced by a stage of quietus and the main events took place in the Asian sector, which is recorded by maximum magmatic activation. During the quietus, weakly consolidated sediments accumulated in the Geofizikov Basin, the Laptev Sea rift system that began to form, and the system of local pull-apart basins connecting them.

CONCLUSIONS

1. Using the apatite fission track method, an age of ~90 Ma was established for the onset of rapid rock exhumation in northeast Franz Josef Land.

2. The obtained age is very close to the beginning of the Late Cretaceous stage ~95 Ma cooling of rocks taken from the slope of the Lomonosov Ridge from the side of the Eurasian Basin opposite western Franz Josef Land.

Based on the interpretation of seismic profile ARC1407A, which intersects the Lomonosov Ridge in the central part, in the lower part of the section, progradation of sediments towards the Amerasian Basin has been established.

The progradation of sediments was caused by Late Cretaceous rock exhumation from the Paleo-Barents–Kara continental margin, which included the future Lomonosov Ridge, which suggests a Cenomanian–Turonian age for the lower part of the prograded sedimentary deposits.

3. The age of rock cooling in the ~95–90 Ma range is widely expressed on the coast of the northern North Atlantic and in the Arctic; the obtained age correlates with the Cenomanian–Coniacian stage of magmatism (~97–89 Ma) on Axel Heiberg Island and Ellesmere Island, part of the Canadian Arctic Archipelago, on the Alpha Ridge, and in the northern part of the Verkhoyansk fold-thrust belt near the coast of the Laptev Sea.

The Cenomanian–Coniacian stage of tectonomagmatic activation is associated with the rifting stage, suggesting that the segmented extension axis passed within:

- the grabens of Melville Bay (Greenland part of Baffin Bay);

- the Axel Heiberg Island and Ellesmere Island;

- the central part of the Alpha Ridge;

- the western part of the Podvodnikov Basin between the Lomonosov Ridge and the Geofizikov spur;

- the system of southwestern grabens of the Laptev Sea and adjacent region of the northern part of the Verkhoyansk fold-thrust belt.

4. The cause of the Cenomanian–Coniacian stage of tectonomagmatic activation was the restructuring of directions of movement of the Pacific plates, which occurred ~95 Ma. This confirms the earlier assumption about the direct influence in the Cretaceous on geodynamic evolution of the Arctic and Northeast Asia and the nature of the subduction regime of the oceanic lithosphere in the northwestern Pacific Ocean.

There is an obvious correlation between the stage of compression of the crust on the Pacific side of North America, which is recorded by magmatism (~119–90 Ma) in the North American Cordillera and activation of rifting in the Labrador Sea–Baffin Bay system.

Movement of the North American Cordillera towards the trench, which began ~125 Ma, led to the emergence of a space between the North American Plate and Greenland, which triggered active rifting in the Labrador Sea–Baffin Bay system. As a result, in addition to the previously formed stretching zone in the eastern North Atlantic, another stretching zone emerged in the western North Atlantic.

ACKNOWLEDGMENTS

The authors thank Corresponding Member of the Russian Academy of Sciences V.V. Akinin (North–East Interdisciplinary Scientific Research Institute, Far Eastern Branch, Russian Academy of Sciences, Magadan, Russia) and Cand. Sci. (Geol.–Mineral.) A.V. Prokopev (Diamond and Precious Metal Geology Institute, Siberian Branch, Russian Academy of Sciences, Yakutsk, Russia) for providing data on magmatism of the Eastern Arctic, and V.I. Petrova (VNIOkeangeologiya, St. Petersburg, Russia) for consultations on the degree of catagenetic transformations of organic matter contained in the of the Severnaya borehole core. The authors are grateful to reviewer A.A. Peive (Geology Institute, Russian Academy of Sciences, Moscow, Russia) and an anonymous reviewer for useful comments and to editor M.N. Shoupletsova (Geology Institute, Russian Academy of Sciences, Moscow, Russia) for careful editing.

FUNDING

The study was supported by the Russian Science Foundation, project no. 22-27-00440 “Construction of Models of the Tectonic Evolution of Sedimentary Basins of the Arctic Zone of Russia Based on Geochronological and Geological-Geophysical Data.”

CONFLICT OF INTEREST

The authors of the work declare that they have no conflicts of interest.

REFERENCES

1. V. V. Abashev, D. V. Metelkin, V. A. Vernikovskiy, E. A. Vasyukova, and N. E. Mikhaltsov, “Early Cretaceous basalts of the Franz Josef Land Archipelago: Correspondence of new $^{40}\text{Ar}/^{39}\text{Ar}$ and paleomagnetic data,” *Dokl. Earth Sci.* **493**, 495–498 (2020).
2. D. Yu. Bol’shiyanov, B. S. Vasil’ev, N. P. Vinogradova, A. V. Gavrish, et al., *The 1 : 1000000 State Geological Map of Russian Federation (3rd ed.). Laptev Sea–Siberian Sea Ser., Sheet S-51–Olenek Bay, S-52–Lena River Delta. Explanatory Note* (Vseross. Nauchno-Issled. Geol. Inst., St. Petersburg, 2014) [in Russian].
3. E. G. Bro, T. M. Pchelina, E. N. Preobrazhenskaya, Z. Z. Ronkina, A. G. Voitsekhovskaya, V. L. Krasnova, and O. V. Mozhaeva, “Sedimentary cover of the Barents Sea shelf on the results of stratigraphic drilling on the islands,” in *Problems of Petroleum Potential of the World Ocean* (Nauka, Moscow, 1989), pp. 191–197.
4. D. A. Vasiliev, A. V. Prokop’ev, A. K. Khudoley, V. B. Ershova, G. G. Kazakova, and E. V. Vetrov, “Thermochronology of the northern part of the Verkhoyansk fold-and-thrust belt according to apatite fission-track age,” *Prirodnye Resursy Arktiki i Subarktkiki* **24** (4), 49–66 (2019). <https://doi.org/10.31242/2618-9712-2019-24-4-4>
5. M. V. Gertseva, T. P. Borisova, E. D. Chibisova, E. N. Emel’yanova, et al., *The 1 : 1000000 State Geological Map of Russian Federation (3rd ed.). Verkhoyansk–Kolyma Ser. Sheet R-52-Tiksi. Explanatory Note* (Vseross. Nauchno-Issled. Geol. Inst., St. Petersburg, 2016) [in Russian].
6. V. Yu. Glebovskiy, V. D. Kaminsky, A. N. Minakov, S. A. Merkur’ev, V. A. Childers, and J. M. Brozina, “Formation of the Eurasia Basin in the Arctic Ocean as inferred from geohistorical analysis of the anomalous magnetic field,” *Geotectonics* **40**, 263–281 (2006).
7. I. S. Gramberg, N. K. Evdokimova, and O. I. Suprunenko, “Catagenetic zonation in sedimentary cover of the Barents shelf: Implication for oil and gas potential,” *Russ. Geol. Geophys.* **42** (11–12), 1808–1820 (2001).
8. I. S. Gramberg, I. V. Shkola, E. G. Bro, V. A. Shekhdanov, and A. M. Armishev, “Parametric boreholes on islands of the Barents and Kara seas,” *Sov. Geol.*, No. 1, 95–98 (1985).
9. A. F. Grachev, “A new view on the origin of magmatism of the Franz Josef Land,” *Izv., Phys. Solid Earth* **37** (9), 744–756 (2001).
10. L. G. Derevyanko, E. A. Gusev, and A. A. Krylov, “Palynological characteristics of cretaceous rocks from the Lomonosov Ridge,” *Problemy Arktiki Antarktiki* **82** (2), 78–84 (2009).
11. V. D. Dibner, *The 1 : 1000000 State Geological Map of Russian Federation. Sheet U/T-38-41 (Frantz Josef Land). Explanatory Note* (Gosgeoltekhizdat, Moscow, 1957).
12. S. S. Drachev, “Tectonics of the Laptev Sea rift system,” *Geotectonics* **34**, 467–481 (2000).
13. V. A. Dymov, N. V. Kachurina, A. A. Makar’ev, E. M. Makar’eva, et al., *The 1 : 1000000 State Geological Map of Russian Federation (New Ser.). Sheet U-37-40 (Frantz Josef Land (Northern Islands)). Explanatory Note*, Ed. by A. A. Makar’ev (Vseross. Nauchno-Issled. Geol. Inst, St. Petersburg, 2006) [in Russian].
14. V. A. Dymov, N. V. Kachurina, A. A. Makar’ev, E. M. Makar’eva, et al., *The 1 : 1000000 State Geological Map of Russian Federation (3rd ed.). North Kara–Kara-Barents Sea Ser. Sheet U-41-44 (Frantz Josef Land (Eastern Islands)). Explanatory Note*, Ed. by A. A. Makar’ev (Vseross. Nauchno-Issled. Geol. Inst, St. Petersburg, 2011) [in Russian].
15. A. M. Karasik, “Magnetic anomalies of the Gakkel Ridge and the origin of the Eurasian Subbasin of the Arctic Ocean,” *Geophysical Survey Methods in the Arctic*, No. 5, 8–19 (1968)
16. Yu. V. Karyakin and E. V. Shipilov, “Geochemical specifics and $^{40}\text{Ar}/^{39}\text{Ar}$ age of the basaltoid magmatism of the Alexander Land, Northbrook, Hooker, and Hayes islands (Franz Josef Land Archipelago),” *Dokl. Earth Sci.* **425** (1), 260–263 (2009).
17. E. A. Korago, N. M. Stolbov, N. N. Sobolev, and A. V. Shmanyak, “Igneous Series in the Eastern Sec-

- tor Islands of Russian Arctic,” in *70 Years in the Arctic, Antarctic, and World Oceans*, Ed. by V. D. Kamirskii, G. P. Avetistov, and V. L. Ivanov (VNIIOkeangeologiya, St. Petersburg, 2018), pp. 101–127 [in Russian].
18. I. N. Kosteva, “Stratigraphy of Jurassic–Cretaceous deposits in the Frantz Josef Land Archipelago,” *Arktika Antarktika* **38** (4), 16–32 (2005).
 19. N. P. Laverov, L. I. Lobkovsky, M. V. Kononov, et al., “A geodynamic model of the evolution of the Arctic basin and adjacent territories in the Mesozoic and Cenozoic and the outer limit of the Russian Continental Shelf,” *Geotectonics* **47**, 1–30 (2013).
<https://doi.org/10.7868/S0016853X13010050>
 20. L. I. Lobkovsky, V. E. Verzhbitsky, M. V. Kononov, et al., “Geodynamic model of the evolution of the Arctic Region in the Late Mesozoic–Cenozoic and the problem of the outer boundary of the continental shelf of Russia,” *Arktika: Ekol. Ekonom.*, No. 1, 104–115 (2011).
 21. L. I. Lobkovsky, M. V. Kononov, and E. V. Shipilov, “Geodynamic causes of the emergence and termination of Cenozoic shear deformations in the Khatanga–Lomonosov Fault Zone (Arctic),” *Dokl. Earth Sci.* **492**, 356–360 (2020).
 22. A. F. Morozov, O. V. Petrov, S. P. Shokalsky, S. N. Kashubin, A. A. Kremenetsky, M. Yu. Shkatov, V. D. Kaminsky, E. A. Gusev, G. E. Grikurov, P. V. Reccant, S. S. Shevchenko, S. A. Sergeev, and V. V. Shatov, “New geological data are confirming continental origin of the Central Arctic Rises,” *Regional. Geol. Metallogen.* No. **53**, 34–55 (2013).
 23. A. M. Nikishin, E. I. Petrov, K. F. Startseva, E. A. Rodina, H. Posamenter, J. Foulger, I. F. Glumov, A. F. Morozov, V. E. Verzhbitsky, N. A. Malyshev, S. I. Freiman, A. P. Afanasenkov, A. V. Bezyazykov, M. S. Doronina, V. A. Nikishin, S. G. Skolotnev, and A. A. Chernykh, “Seismostratigraphy, paleogeography and paleotectonics of the Arctic deep-water basin and its Russian shelf zones,” in *Transactions of Geological Institute of Russian Academy of Sciences, Vol. 632*, Ed. by N. B. Kuznetsov (GEOS, Moscow, 2022).
 24. A. A. Peyve, “Similarity and differences of Cretaceous magmatism in the Arctic Region,” *Geotectonics* **52**, 194–208 (2018).
 25. V. I. Petrova, G. I. Batova, A. V. Kursheva, I. V. Litvinenko, and I. P. Morgunova, “Molecular geochemistry of organic matter of Triassic rocks in the north-eastern part of the Barents Sea: The influence of tectonic and magmatic processes,” *Russ. Geol. Geophys.* **58** (3–4), 322–331 (2017).
 26. V. A. Poselov, G. P. Avetisov, V. V. Butsenko, S. M. Zhondz, V. D. Kaminsky, and S. Pavlov, “The Lomonosov Ridge as a natural extension of the Eurasian continental margin into the Arctic Basin,” *Russ. Geol. Geophys.* **53** (12), 1276–1290 (2012).
 27. E. N. Preobrazhenskaya, I. B. Shkola, and M. V. Korchinskaya, “Stratigraphy of Triassic sediments in the Franz Josef Land Archipelago (based on parametric drilling),” in *Stratigraphy and Paleontology of Mesozoic Sedimentary Basins in the Northern Soviet Union*, Ed. By. N. D. Vasilevskaya (Sevmorgeologiya, Leningrad, 1985), pp. 42–64.
 28. V. F. Proskurnin, A. V. Gavrish, V. V. Mezhubovsky, V. R. Trofimov, et al., *The 1 : 1000000 State Geological Map of the Russian Federation (3rd ed.). Ser. Taimyr–Severnaya Zemlya. Sheet S-49 (Khatanga Bay). Explanatory Note* (Vseross. Nauchno-Issled. Geol. Inst., St. Petersburg, 2013).
 29. V. F. Proskurnin, S. I. Shkarubo, G. A. Zavarzina, N. I. Nagaitseva, et al., *The 1 : 1000000 State Geological Map of the Russian Federation (3rd ed.). Ser. Laptev Sea–Siberian Sea. Sheet S-50 (Ust-Olenek). Explanatory Note* (Vseross. Nauchno-Issled. Geol. Inst., St. Petersburg, 2017).
 30. Yu. S. Repin, A. A. Fedorova, V. V. Bystrova, et al., “Mesozoic of the Barents Sea sedimentation basin,” in *Stratigraphy and Its Significance for the Russian Oil and Gas Industry*. (VNIGRI, St. Petersburg, 2007), pp. 112–161.
 31. S. G. Skolotnev, M. A. Fedonkin, and A. V. Korniychuk, “New data on the age of magmatic rocks in the Alpha–Mendeleev Rise (Arctic Ocean) Based on the results of isotope U/Pb dating of zircons,” *Dokl. Earth Sci.* **513**, 1104–1109 (2023).
 32. S. D. Sokolov and L. I. Lobkovsky, “Tectonic models of the formation of the Arctic margins of Chukotka and Northern Alaska: From ocean to collision,” in *Proceedings of LIV Tectonic Conference “Tectonics and Geodynamics of the Earth’s crust and Mantle: Fundamental problems,” Moscow, January 2023*, Ed. by K. E. Degtyarev (GEOS, Moscow, 2023), vol. 2, pp. 203–206, 2023.
 33. A. V. Soloviev, A. V. Zaionchek, O. I. Suprunenko, H. Brekke, J. I. Faleide, D. V. Rozhkova, A. I. Khisamutdinova, N. M. Stolbov, and J. K. Hourigan, “Evolution of the provenances of Triassic rocks in Franz Josef Land: U/Pb LA-ICP-MS dating of the detrital zircon from Well Severnaya,” *Lithol. Miner. Resour.* **50**, 102–116 (2015).
 34. S. G. Skolotnev, M. A. Fedonkin, and A. V. Korniychuk, “New data on the geological structure of the southwestern Mendeleev Rise, Arctic Ocean,” *Dokl. Earth Sci.* **476** (1), 1001–1006 (2017).
 35. N. M. Stolbov, Candidate’s Dissertation in Geology and Mineralogy (St. Petersburg. State Univ., St. Petersburg, 2005).
 36. A. N. Tarakhovskiy, M. V. Fishman, I. V. Shkola, and V. L. Andreichev, “The age of traps of the Frantz Josef Land Archipelago,” *Dokl. Akad. Nauk SSSR* **266** (4), 965–969 (1982).
 37. E. V. Shipilov and Yu. V. Karyakin, “Dikes of Hayes Island (Frantz Josef Land Archipelago): Tectonic position and geodynamic interpretation,” *Dokl. Earth Sci.* **457**, 814–818 (2014).
 38. V. V. Akinin, E. L. Miller, J. Toro, A. V. Prokopiev, E. S. Gottlieb, S. Pearcey, G. O. Polzunenkov, and V. A. Trunilina, “Episodicity and the dance of Late Mesozoic magmatism and deformation along the northern circum-Pacific margin: North-eastern Russia to the Cordillera,” *Earth-Sci. Rev.* **208**, Art.103272, 2020.
<https://doi.org/10.1016/j.earscirev.2020.103272>
 39. S. Alsulami, D. A. Paton, and D. G. Cornwell, “Tectonic variation and structural evolution of the West Greenland continental margin,” *AAPG Bull.* **99** (9), 1689–1711 (2015).

40. T. Altenbernd, W. Jokat, I. Heyde, and V. Damm, "A crustal model for northern Melville Bay, Baffin Bay," *J. Geophys. Res. Solid Earth* **119**, 8610–8632 (2014), <https://doi.org/10.1002/2014JB011559>
41. A. Alvey, C. Gaina, N. J. Kusznir, and T. H. Torsvik, "Integrated crustal thickness mapping and plate reconstructions for the high Arctic," *Earth Planet. Sci. Lett.* **274**, 310–321 (2008).
42. J. M. Amato, J. E. Wright, P. B. Gans, and E. L. Miller, "Magmatically induced metamorphism and deformation in the Kigluaik gneiss dome, Seward Peninsula, Alaska," *Tectonics* **13**, 515–527 (1994). <https://doi.org/10.1029/93TC03320>
43. J. Backman, M. Jakobsson, M. Frank, F. Sangiorgi, H. Brinkhuis, C. Stickley, M. O'Regan, R. Lovlie, H. Palike, D. Spofforth, J. Gattacecca, K. Moran, J. King, and C. Heil, "Age model and core-seismic integration for the Cenozoic ACEX sediments from the Lomonosov Ridge," *Paleoceanography* **23**, 1–15 (2008). <https://doi.org/10.1029/2007PA001476>
44. J. Backman, K. Moran, D. B. McInroy, L. A. Mayer, and the Expedition 302 Scientists, *IODP-302* (Proc. IODP – Integrated Ocean Drilling Program Management International, Edinburgh, 2006, Vol. 302). <https://doi.org/10.2204/iodp.proc.302.101.2006>
45. N. Barnett-Moore, D. R. Muller, S. Williams, J. Skogseid, and M. Seton, "A reconstruction of the North Atlantic since the earliest Jurassic," *Basin Res.* **30** (Suppl. 1), 160–185 (2018). <https://doi.org/10.1111/bre.12214>
46. S. Bonvalot, G. Balmino, A. Briais, M. Kuhn, A. Peyrefitte, N. Vales, R. Biancale, G. Gabalda, F. Reinquin, and M. Sarrailh, *World Gravity Map (Commission for the Geological Map of the World, 2012)*, (BGI-CGMW-CNES-IRD, Paris). <https://ccgm.free.fr/>
47. H. Brekke, "The tectonic evolution of the Norwegian Sea continental margin, with emphasis on the Voring and More basins," *Spec. Publ.—Geol. Soc. London*, No. 167, 327–378 (2000).
48. J. M. Brozena, V. A. Childers, L. A. Lawver, L. M. Gahagan, J. I. Forsberg, J. I. Faleide, and O. Eldholm, "New aerogeophysical study of the Eurasia Basin and Lomonosov Ridge: implications for basin development," *Geology* **31** (9), 825–828 (2003).
49. K. Brumley, *Geologic History of the Chukchi Borderland, Arctic Ocean. PhD Thesis* (Stanford University, CA, 2014).
50. S. E. Bryan, I. U. Peate, D. W. Peate, D. A. Jerram, M. R. Mawby, J. S. Marsh, and J. A. Miller, "The largest volcanic eruptions on Earth," *Earth Sci. Rev.* **192** (3–4), 207–229 (2010). <https://doi.org/10.1016/j.earscirev.2010.07.001>
51. J. A. Chalmers and T. C. R. Pulvertaft, "Development of the continental margins of the Labrador Sea: A review," in *Non-volcanic Rifting of Continental Margins: A Comparison of Evidences from Land and Sea*, Ed. by R. C. L. Wilson, R. B. Whitmarsh, B. Taylor, and N. Froitzheim (Spec. Publ.—Geol. Soc. London, 2001), pp. 77–105.
52. D. Chardon, "Strain partitioning and batholith emplacement at the root of a transpressive magmatic arc," *J. Struct. Geol.* **25**, 91–108 (2003).
53. R. L. Christie, "Tertiary rocks at Lake Hazen, northern Ellesmere Island," *Geol. Surv. Can.*, No. 76–1B, 259–262 (1976).
54. B. Coakley, K. Brumley, N. Lebedeva-Ivanova, and D. Mosher, "Exploring the geology of the central Arctic Ocean; understanding the basin features in place and time," *J. Geol. Soc. London* **173**, 967–987 (2016). <https://doi.org/10.1144/jgs2016-082>
55. J. Cochran, M. Edwards, and B. Coakley, "Morphology and structure of the Lomonosov Ridge, Arctic Ocean," *Geochem., Geophys., Geosyst.* **7**, Art. Q05019 (2006). <https://doi.org/10.1029/2005GC001114>
56. M. F. Coffin and O. Eldholm, "Large Igneous Provinces—Crustal structure, dimensions and external consequences," *Rev. Geophys.* **32** (1), 1–36 (1994).
57. K. M. Cohen, S. C. Finney, P. L. Gibbard, and J.-X. Fan, "The ICS International Chronostratigraphic Chart," *Episodes* (36), 199–204 (2013).
58. F. Corfu, S. Polteau, S. Planke, J. I. Faleide, H. Svensen, A. Zayoncheck, and N. Stolbov, "U–Pb geochronology of Cretaceous magmatism on Svalbard and Franz Josef Land, Barents Sea Large Igneous Province," *Geol. Mag.* **150** (6), 1127–1135 (2013).
59. V. D. Dibner, "The Geology of Franz Jozef Land – an introduction," in *Geological Aspects of Franz Josef Land and the Northernmost Barents Sea. The Northern Barents Sea Geotraverse*, Ed. by A. Solheim, E. Musatov, and N. Heintz (Norsk Polarinst. Meddelelser, Oslo, Norway, 1998), vol. 151, pp. 10–117.
60. V. D. Dibner, V. L. Andreichev, A. N. Tarakhovsky, and I. V. Shkola, "Timing of plateau basalts," in *Geology of Franz Jozef Land*, Ed. by V. D. Dibner (Norsk Polarinst. Meddelelser, Oslo, Norway, 1998), vol. 146.
61. D. M. Dockman, D. G. Pearson, L. M. Heaman, S. A. Gibson, and C. Sarkar, "Timing and origin of magmatism in the Sverdrup Basin, Northern Canada—implications for lithospheric evolution in the High Arctic Large Igneous Province (HALIP)," *Tectonophysics* **742–743** 50–65 (2018). <https://doi.org/10.1016/j.tecto.2018.05.010>
62. R. A. Donelick and D. S. Miller, "Enhanced TINT fission track densities in low spontaneous track density apatites using 252Cf-derived fission fragment tracks: A model and experimental observations," *Nuclear Tracks Radiation Measurements* **18**, 301–307 (1991).
63. R. A. Donelick, P. B. O'Sullivan, and R. A. Ketcham, "Apatite fission-track analysis," *Rev. Mineral. Geochem.* **58**, 49–94 (2005).
64. A. Dore, "The structural foundation and evolution of Mesozoic seaways between Europe and Arctic," *Palaeogeogr., Palaeoclimatol., Palaeoecol.* **87** 441–492 (1991).
65. A. G. Dore, E. R. Lundin, A. Gibbons, T. O. Somme, and B. O. Torudbakken, "Transform margins of the Arctic: A synthesis and re-evaluation," in *Transform Margins: Development, Controls and Petroleum Systems*, Ed. by M. Nemcok, S. Rybar, S. T. Sinha, S. A. Hermeton, and L. Ledvenyiove (Spec. Publ.—Geol. Soc. London, 2016, Vol. 431), pp. 63–94. <https://doi.org/10.1144/SP431.8>
66. N. Dorr, F. Lisker, P. D. Clift, A. Carter, D. G. Gee, A. M. Tebenkov, and C. Spiegel, "Late Mesozoic

- Cenozoic exhumation history of northern Svalbard and its regional significance: Constraints from apatite fission track analysis,” *Tectonophysics* **514–517** 81–92 (2012).
<https://doi.org/10.1016/j.tecto.2011.10.007>
67. N. Dorr, F. Lisker, K. Piepjohn, and C. Spiegel, “Cenozoic development of northern Svalbard based on thermochronological data,” *Terra Nova* **31** (3), 306–315 (2019).
<https://doi.org/10.1111/ter.12402>
 68. A. Døssing, J. Hopper, A. Olesen, and J. Halpenny, “New aero-geophysical results from the Arctic Ocean, north of Greenland: Implications for Late Cretaceous rifting and Eureka compression,” *Geochem., Geophys., Geosyst.* **14** (10), 4044–4065 (2013).
 69. S. S. Drachev, N. A. Malyshev, and A. M. Nikishin, “Tectonic history and petroleum geology of the Russian Arctic Shelves: An overview,” in *Proceedings of the 7th Petroleum Geology Conference “Petroleum Geology: From Mature Basins to New Frontiers”*, Ed. by B. A. Vining and S. C. Pickering (Geol. Soc. London, 2010), pp. 591–619.
<https://doi.org/10.1144/0070591>
 70. S. S. Drachev and S. I. Shkarubo, “Tectonics of the Laptev Shelf, Siberian Arctic,” in *Circum-Arctic Lithosphere Evolution*, Ed. by V. Pease and B. Coakley (Spec. Publ.—Geol. Soc. London, 2018, Vol. 460), pp. 263–283.
<https://doi.org/10.1144/sp460.15>
 71. H. Dypvik, B. Fjellsa, T. Pcelina, A. Sokolov, and A. Raheim, “The diagenetic of the Triassic succession of Franz Josef Land,” in *Geological Aspects of Franz Josef Land and the Northernmost Barents Sea. The Northern Barents Sea Geotraverse*, Ed. by A. Solheim, E. Musatov, and N. Heintz (Norsk Polarinst. Meddelelser, Oslo, Norway, 1998), vol. 151, pp. 83–104.
 72. H. Dypvik, A. Sokolov, T. Pcelina, B. Fjellsa, T. Bjærke, M. Korchinskaya, and J. Nagy, “The Triassic succession of the Franz Josef Land, stratigraphy and sedimentology of three wells from Alexandra, Hayes and Graham Bell Islands,” in *Geological Aspects of Franz Josef Land and the Northernmost Barents Sea. The Northern Barents Sea Geotraverse*, Ed. by A. Solheim, E. Musatov, and N. Heintz (Norsk Polarinst. Meddelelser, Oslo, Norway, 1998), vol. 151, pp. 50–82.
 73. T. A. Dumitru, “A new computer-automated microscope stage system for fission track analysis,” *Nuclear Tracks Radiation Measurements*, **21**, 575–580 (1993).
 74. T. A. Dumitru, “Fission-track geochronology,” in *Quaternary Geochronology: Methods and Applications*, Ed. by J. S. Noller, J. M. Sowers, and W. R. Lettis (AGU, Geophys. Monogr. Ser., AGU Reference Shelf 4, Washington, D.C., USA, 2000), pp. 131–155.
<https://doi.org/10.1029/RF004p0131>
 75. O. Eldholm and M. F. Coffin, “Large igneous provinces and plate tectonics,” in *The History and Dynamics of Global Plate Motions*, Ed. by M. A. Richards, R. G. Gordon, and R. D. van der Hilst (AGU, Washington, D.C., USA, 2000), pp. 309–326.
<https://doi.org/10.1029/GM121p0309>
 76. A. F. Embry, “Mesozoic history of the Arctic Islands,” in *Geology of the Innuitian Orogen and Arctic Platform of Canada and Greenland*, Ed. by H. P. Trettin (Boulder, Colorado. GSA, Geology of North America. Vol. E), pp. 369–433.
 77. A. F. Embry and K. G. Osadetz, “Stratigraphy and tectonic significance of Cretaceous volcanism in the Queen Elizabeth Islands, Canadian Arctic Archipelago,” *Can. J. Earth Sci.* **25**, 1209–1219 (1988).
 78. R. E. Ernst, *Large Igneous Provinces* (Cambridge Univ. Press, London, 2014).
<https://doi.org/10.1017/CBO9781139025300>
 79. S. Estrada, “Geochemical and Sr–Nd isotope variations within Cretaceous continental flood-basalt suites of the Canadian High Arctic, with a focus on the Hassel Formation basalts of northeast Ellesmere Island,” *Int. J. Earth Sci.* **104** (8), 1981–2005 (2015).
 80. S. Estrada and F. Henjes-Kunst, “⁴⁰Ar–³⁹Ar and U–Pb dating of Cretaceous continental rift-related magmatism on the northeast Canadian Arctic margin,” *Z. Dtsch. Ges. Geowiss.* **164**, 107–130 (2013).
 81. J. Evangelatos, T. Funck, and D. C. Mosher, “The sedimentary and crustal velocity structure of Makarov Basin and adjacent Alpha Ridge,” *Tectonophysics* **696–697** 99–114 (2017).
<https://doi.org/10.1016/j.tecto.2016.12.026>
 82. J. I. Faleide, K. Bjørlykke, and R. H. Gabrielsen, “Geology of the Norwegian Continental Shelf,” in *Petroleum Geoscience*, Ed. by K. Bjørlykke (Springer, Berlin–Heidelberg, 2015), pp. 467–499.
https://doi.org/10.1007/978-3-642-34132-8_25
 83. J. I. Faleide, F. Tsikalas, A. J. Breivik, R. Mjelde, O. Ritzmann, Ø. Engen, J. Wilson, and O. Eldholm, “Structure and evolution of the continental margin off Norway and the Barents Sea,” *Episodes* **31** 82–91 (2008).
 84. P. G. Fitzgerald and A. J. W. Gleadow, “New approaches in fission track geochronology as a tectonic tool: Examples from the Transantarctic Mountains,” *Nuclear Tracks Radiation Measurements* **17** (3), 351–357 (1990).
[https://doi.org/10.1016/1359-0189\(90\)90057-5](https://doi.org/10.1016/1359-0189(90)90057-5)
 85. P. G. Fitzgerald and M. G. Malusà, “Concept of the exhumed partial annealing (retention) zone and age-elevation profiles in thermochronology,” in *Fission-Track Thermochronology and Its Application to Geology*, Ed. by M. G. Malusà and P. G. Fitzgerald (Springer Textbooks in Earth Sci., Geogr. Environ., Berlin, Germany, 2019), pp. 165–189.
https://doi.org/10.1007/978-3-319-89421-8_9
 86. P. G. Fitzgerald, R. B. Sorkhabi, T. F. Redfield, and E. Stump, “Uplift and denudation of the central Alaska Range; a case study in the use of apatite fission track thermochronology to determine absolute uplift parameters,” *J. Geophys. Res.* **100**, 20175–20191 (1995).
 87. C. Gaina, L. Gernigon, and P. Ball, “Paleocene–recent plate boundaries in the NE Atlantic and the formation of the Jan Mayen microcontinent,” *J. Geol. Soc.* **166** (4), 601–616 (2009).
 88. C. Gaina, W. R. Roest, and R. D. Müller, “Late Cretaceous–Cenozoic deformation of northeast Asia,” *Earth Planet. Sci. Lett.* **197**, 273–286 (2002).
 89. R. F. Galbraith, “On statistical models for fission track counts,” *Math. Geol.* **13**, 471–478 (1981).

90. R. F. Galbraith and G. M. Laslett, "Statistical models for mixed fission track ages," *Nuclear Tracks Radiation Measurements* **21** 459–470 (1993).
91. K. Gallagher, R. Brown, and C. Johnson, "Fission track analysis and its applications to geological problems," *Ann. Rev. Earth Planet. Sci.* **26**, 519–572 (1998).
92. L. Gernigon, D. Franke, L. Geoffroy, C. Schiffer, G. R. Foulger, and M. Stoker, "Crustal fragmentation, magmatism, and the diachronous opening of the Norwegian–Greenland Sea," *Earth-Sci. Rev.* **206**, Art. 102839 (2020).
<https://doi.org/10.1016/j.earscirev.2019.04.01110.1016>
93. A. J. W. Gleadow, I. R. Duddy, P. F. Green, and J. F. Lovering, "Confined fission track lengths in apatite: A diagnostic tool for thermal history analysis," *Contrib. Mineral. Petrol.* **94** (4), 405–415 (1986).
<https://doi.org/10.1007/BF00376334>
94. E. S. Gottlieb, E. L. Miller, A. Andronikov, K. Brumley, L. A. Mayer, and S. B. Mukasa, "Cretaceous Arctic magmatism: Slab vs. plume? Or slab and plume?" in *AGU Fall Meeting. San-Francisco, CA, USA, December 13–17, 2010. Abstr. T31A-2139*.
95. A. F. Grachev, "Geodynamics of the transitional zone from the Moma Rift to the Gakkel Ridge," in *Studies in Continental Margin Geology*, Ed. by J. S. Watkins and C. L. Drake, *Am. Assoc. Petrol. Geol. Mem.* **34**, 103–114 (1983).
96. A. F. Grachev, M. M. Arakelyantz, V. A. Lebedev, E. E. Musatov, and N. M. Stolbov, "New K–Ar ages for basalts from Franz Josef Land," *Rus. J. Earth Sci.* **3**, 79–82 (2001).
97. W. H. Craddock and D. W. Houseknecht, "Cretaceous–Cenozoic burial and exhumation history of the Chukchi shelf, offshore Arctic Alaska," *Am. Assoc. Pet. Geol. Bull.*, No. 100, 63–100 (2016).
<https://doi.org/10.1306/09291515010>
98. P. F. Green, "A new look at statistics in fission-track dating," *Nuclear Tracks Radiation Measurements* **5**, 77–86 (1981)
99. P. F. Green, I. R. Duddy, A. J. W. Gleadow, and J. F. Lovering, "Apatite fission-track analysis as a paleotemperature indicator for hydrocarbon exploration," in *Thermal History of Sedimentary Basins: Methods and Case Histories*, Ed. by N. D. Naeser and T. N. McCulloh (Springer, NY, DC, USA, 1989), pp. 181–195.
https://doi.org/10.1007/978-1-4612-3492-0_11
100. U. Gregersen, J. R. Hopper, and P. C. Knutz, "Basin seismic stratigraphy and aspects of prospectivity in the NE Baffin Bay, Northwest Greenland," *Mar. Petrol. Geol.* **46**, 1–18 (2013).
101. A. M. Grist and M. Zentilli, "The thermal history of the Nares Strait, Kane Basin, and Smith Sound region in Canada and Greenland: constraints from apatite fission-track and (U–Th–Sm)/He dating," *Can. J. Earth Sci.* **42**, 1547–1569 (2005).
<https://doi.org/10.1139/e05-058>
102. J. C. Harrison, T. A. Brent, and G. N. Oakey, "Baffin Fan and its inverted rift system of Arctic Eastern Canada: Stratigraphy, tectonics and petroleum resource potential," *Geol. Soc. Mem.* **35**, 595–626 (2011).
<https://doi.org/10.1144/M35.40>
103. N. Hasebe, J. Barbarand, K. Jarvis, A. Carter, and A. J. Hurford, "Apatite fission-track chronometry using laser ablation ICP-MS," *Chem. Geol.* **207**, 135–145 (2004).
104. T. X. Homza and S. C. Bergman, "A Geologic interpretation of the Chukchi Sea petroleum province: Offshore Alaska, USA," *Am. Ass. Petrol. Geol.* **119** (2019).
<https://doi.org/10.1306/AAPG119>
105. M. Hosseinpour, R. D. Muller, S. E. Williams, and J. M. Whittaker, "Full-fit reconstruction of the Labrador Sea and Baffin Bay," *Solid Earth.* **4**, 461–479 (2013).
<https://doi.org/10.5194/se-4-461-2013>
106. A. J. Hurford and P. F. Green, "The zeta age calibration of fission-track dating," *Chem. Geol.* **41**, 285–317 (1983).
107. H. R. Jackson, K. Dickie, and F. Marillier, "A seismic reflection study of northern Baffin Bay: implication for tectonic evolution," *Can. J. Earth Sci.* **29** (11), 2353–2369 (1992).
108. H. R. Jackson, P. J. Mudie, and S. M. Blasco, "Initial geological report on CESAR: The Canadian Expedition to Study the Alpha Ridge," *Geol. Surv. Can.*, Pap. 84-22, 59–99 (1985).
109. P. Japsen, P. F. Green, and J. A. Chalmers, "Thermotectonic development of the Wandel Sea Basin, North Greenland," *GEUS Bull.* **45** (2), Art. 5298 (2021).
<https://doi.org/10.34194/geusb.v45.5298>
110. P. Japsen, P. F. Green, J. M. Bonow, M. Bjerager, and J. R. Hopper, "Episodic burial and exhumation in North-East Greenland before and after opening of the North-East Atlantic," *GEUS Bull.* **45** (2), Art. 5299 (2021).
<https://doi.org/10.34194/geusb.v45.5299>
111. M. Jakobsson, L. A. Mayer, C. Bringensparr, et al., "The International Bathymetric Chart of the Arctic Ocean, Version 4.0," *Scientific Data*, Art. **176** (2020).
<https://doi.org/10.1038/s41597-020-0520-9>
112. W. Jokat, "The sedimentary structure of the Lomonosov Ridge between 88° N and 80° N," *Geophys. J. Int.* **163** 698–726 (2005).
113. W. Jokat and M. Ickrath, "Structure of ridges and basins off East Siberia along 81 degrees N, Arctic Ocean," *Mar. Petrol. Geol.* **64**, 222–232 (2015).
114. W. Jokat, M. Ickrath, and J. O'Connor, "Seismic transect across the Lomonosov and Mendeleev Ridges: Constraints on the geological evolution of the Amerasia Basin, Arctic Ocean," *Geophys. Res. Lett.* **40** (19), 5047–5051 (2013).
115. W. Jokat, G. Uenzelmann-Neben, Y. Kristoffersen, and T. M. Rasmussen, "Lomonosov Ridge—A double-sided continental margin," *Geology* **20**, 887–890 (1992).
116. W. Jokat, E. Weigelt, Y. Kristoffersen, T. Rasmussen, and T. Schöne, "New insights into the evolution of the Lomonosov Ridge and the Eurasia Basin," *Geophys. J. Int.* **122**, 378–392 (1995).
117. R. A. Ketcham, A. Carter, R. A. Donelick, J. Barbarand, and A. J. Hurford, "Improved modeling of fission-track annealing in apatite," *Am. Mineral.* **92**, 799–810 (2007).
<https://doi.org/10.2138/am.2007.2281>

118. C. G. Kingsbury, L. K. Sandra, E. E. Richard, U. Soderlund, and B. L. Cousens, "U–Pb geochronology of the plumbing system associated with the Late Cretaceous Strand Fiord Formation, Axel Heiberg Island, Canada: Part of the 130–90 Ma High Arctic large igneous province," *J. Geodynam.* **118**, 106–117 (2017). <https://doi.org/10.1016/j.jog.2017.11.001>
119. C. Knudsen, J. R. Hopper, P. R. Bierman, M. Bjerager, T. Funck, P. F. Green, J. R. Ineson, P. Japsen, C. Marcussen, S. C. Sherlock, and T. B. Thomsen, "Samples from Lomonosov Ridge place new constraints on the geological evolution of Arctic Ocean, in *Circum-Arctic Lithosphere Evolution*, Ed. by V. Pease and B. Coakley (Spec. Publ.—Geol. Soc. London, 2018, Vol. 460), pp. 397–418. <https://doi.org/10.1144/SP460.17>
120. K. L. Kleinspehn and C. Teyssier, "Oblique rifting and the Late Eocene–Oligocene demise of Laurasia with inception of Molloy Ridge: Deformation of Forlandsundet Basin, Svalbard," *Tectonophysics* **693**, 363–377 (2016). <https://doi.org/10.1016/j.tecto.2016.05.010>
121. Y. Kristoffersen, B. J. Coakley, J. K. Hall, and M. Edwards, "Mass wasting on the submarine Lomonosov Ridge, central Arctic Ocean," *Mar. Geol.* **243**, 132–142 (2007).
122. Y. Kristoffersen, H. E. Nilsen, and J. K. Hall, "The High Arctic Large Igneous Province: first seismic-stratigraphic evidence for multiple Mesozoic volcanic pulses on the Lomonosov Ridge, central Arctic Ocean," *J. Geol. Soc.* **180** (5), 1–17 (2023). <https://doi.org/10.1144/jgs2022-153>
123. L. M. Larsen, L. M. Heaman, R. A. Creaser, R. A. Duncan, R. Frei, and M. Hutchison, "Tectonomagmatic events during stretching and basin formation in the Labrador Sea and the Davis Strait: Evidence from age and composition of Mesozoic to Palaeogene dyke swarms in West Greenland," *J. Geol. Soc.* **166**, 999–1012 (2009).
124. G. M. Laslett, W. S. Kendall, A. J. W. Gleadow, and I. R. Duddy, "Bias in the measurement of fission track length distributions," *Nuclear Tracks Radiation Measurements* **6**, 79–85 (1982).
125. K. Matthews, K. T. Maloney, S. Zahirovic, S. E. Williams, M. Seton, and R. D. Müller, "Global plate boundary evolution and kinematics since the late Paleozoic," *Global Planet. Change* **146**, 226–250 (2016). <https://doi.org/10.1016/j.gloplacha.2016.10.002>
126. A. D. Miall, "Late Cretaceous and Tertiary basin development and sedimentation, Arctic Islands," in *Geology of the Inuitian Orogen and Arctic Platform of Canada and Greenland*, Vol. 3. *Geology of Canada*, Ed. by H. P. Trettin (Geol. Surv. Canada, 1991), pp. 437–458. <https://doi.org/10.1130/DNAG-GNA-E.435>
127. E. L. Miller, V. V. Akinin, T. A. Dumitru, E. S. Gottlieb, M. Grove, K. Meisling, and G. Seward, "Deformational history and thermochronology of Wrangel Island, East Siberian Shelf and coastal Chukotka, Arctic Russia," in *Circum-Arctic Lithosphere Evolution*, Ed. by V. Pease and B. Coakley (Spec. Publ.—Geol. Soc. London, 2018, Vol. 460), pp. 207–238. <https://doi.org/10.1144/SP460.7>
128. E. L. Miller, K. E. Meisling, V. V. Akinin, K. Brumley, B. J. Coakley, E. S. Gottlieb, C. W. Hoiland, T. M. O'Brien, A. Soboleva, and J. Toro, "Circum-Arctic Lithosphere Evolution (CALE) Transect C: displacement of the Arctic Alaska–Chukotka microplate towards the Pacific during opening of the Amerasia Basin of the Arctic, in *Circum-Arctic Lithosphere Evolution*, Ed. by V. Pease and B. Coakley (Spec. Publ.—Geol. Soc. London, 2018, Vol. 460), pp. 57–120. <https://doi.org/10.1144/SP460.9>
129. E. L. Miller and V. E. Verzhbitsky, "Structural studies near Pevek, Russia: implications for formation of the East Siberian Shelf and Makarov Basin of the Arctic Ocean," *Stephan Mueller Spec. Publ., Ser. 4*, 2009, pp. 223–241. <https://doi.org/10.5194/smsps-4-223-2009>
130. J. W. H. Monger and H. D. Gibson, "Mesozoic–Cenozoic deformation in the Canadian Cordillera: The record of a "Continental Bulldozer"?", *Tectonophysics* **757**, 153–169 (2019). <https://doi.org/10.1016/j.tecto.2018.12.023>
131. J. W. H. Monger, R. A. Price, and D. J. Tempelman-Kluit, "Tectonic accretion and the origin of the two major metamorphic and plutonic belts in the Canadian Cordillera," *Geology* **10**, 70–75 (1982). [https://doi.org/10.1130/0091-7613\(1982\)10<70:TAA-TOO>2](https://doi.org/10.1130/0091-7613(1982)10<70:TAA-TOO>2)
132. S. B. Mukasa, A. Andronikov, K. Brumley, L. A. Mayer, and A. Armstrong, "Basalts from the Chukchi borderland: $^{40}\text{Ar}/^{39}\text{Ar}$ ages and geochemistry of submarine intraplate lavas dredged from the western Arctic Ocean," *J. Geophys. Res.: Solid Earth* **125**, Art. e2019JB017604 (2020). <https://doi.org/10.1029/2019JB017604>
133. R. D. Muller, M. Seton, S. Zahirovic, S. E. Williams, K. J. Matthews, N. M. Wright, et al., "Ocean basin evolution and global scale plate reorganization events since Pangea breakup," *Ann. Rev. Earth Planet. Sci.* **44** (1), 107–138 (2016). <https://doi.org/10.1146/annurev-earth-060115-012211>
134. J. L. Nelson, M. Colpron, and S. Israel, "The Cordillera of British Columbia, Yukon, and Alaska: Tectonics and metallogeny," *Soc. Econ. Geol.*, pp. 53–109 (2013). <https://doi.org/10.5382/SP.17.03>
135. A. M. Nikishin, C. Gaina, E. I. Petrov, et al., "Eurasia Basin and Gakkel Ridge, Arctic Ocean: Crustal asymmetry, ultra-slow spreading and continental rifting revealed by new seismic data," *Tectonophysics* **746**, 64–82 (2018).
136. A. M. Nikishin, E. I. Petrov, N. A. Malyshev, and V. P. Ershova, "Rift systems of the Russian Eastern Arctic shelf and Arctic deep water basins: Link of geological history and geodynamics," *Geodynam. Tectonophys.* **8** (1), 11–43 (2017). <https://doi.org/10.5800/GT-2017-8-1-0231>
137. A. M. Nikishin, E. A. Rodina, K. F. Startseva, G. R. Foulger, H. W. Posamentier, A. P. Afanasenkov, A. V. Beziazykov, A. A. Chernykh, E. I. Petrov, S. G. Skolotnev, V. E. Verzhbitsky, and I. V. Yakovenko, "Alpha–Mendeleev Rise, Arctic Ocean: A double volcanic passive margin," *Gondwana Res.* **120**, 85–110 (2023). <https://doi.org/10.1016/j.gr.2022.10.010>

138. G. N. Oakey and J. A. Chalmers, “A new model for the Paleogene motion of Greenland relative to North America: Plate reconstructions of the Davis Strait and Nares Strait regions between Canada and Greenland,” *J. Geophys. Res. Ser. B: Solid Earth* **117**, Art. B10401 (2012).
<https://doi.org/10.1029/2011JB008942>
139. G. N. Oakey and R. W. Saltus, “Geophysical analysis of the Alpha–Mendeleev Ridge complex: Characterization of the high Arctic large Igneous Province,” *Tectonophysics* **691**, 65–84 (2016).
<https://doi.org/10.1016/j.tecto.2016.08.005>
140. G. N. Oakey and R. A. Stephenson, “Crustal structure of the Inuitian region of Arctic Canada and Greenland from gravity modelling: Implications for the Palaeogene Eurekan Orogen,” *Geophys. J. Int.* **173** (3), 1039–1063 (2008).
141. A. V. Okulitch and H. P. Trettin, “Late Cretaceous–Early Tertiary deformation, Arctic Islands,” in *Geology of the Inuitian Orogen and Arctic Platform of Canada and Greenland*, Ed. by H. P. Trettin (Geol. Surv. Can. Ottawa, Ontario, 1991, Vol. 3, Ch. 17), pp. 467–489.
142. K. G. Osadetz and P. R. Moore, “Basic volcanics in the Hassel Formation (Mid-Cretaceous) and associated intrusives, Ellesmere Island, District of Franklin, Northwest Territories,” *Geol. Surv. Can.*, Pap. 87–21, 1–19 (1988).
143. K. Piejohn, W. von Gosen, and F. Tessensohn, “The Eurekan deformation in the Arctic: An outline,” *J. Geol. Soc.* **173** (6), 1007–1024 (2016).
<https://doi.org/10.1144/jgs2016-081>
144. S. M. Phillips, “Deformation in a shear zone, Central Ellesmere Island, Canadian Arctic Archipelago: Implications for regional tectonics,” *Mar. Geol.* **93**, 385–400 (1990).
145. S. Polteau, B. W. H. Hendriks, S. Planke, M. Ganerød, F. Corfu, J. I. Faleide, et al., “The early cretaceous Barents Sea sill complex: Distribution, $^{40}\text{Ar}/^{39}\text{Ar}$ geochronology, and implications for carbon gas formation,” *Palaeogeogr., Palaeoclimatol., Palaeoecol.* **441**, 83–95 (2016).
<https://doi.org/10.1016/j.palaeo.2015.07.007>
146. S. Planke, J. Christensen, S. Polteau, and R. Myklebust, “Mid-Cretaceous source rock subcropping in the Baffin Bay,” *GEO ExPro* **6**, 6–8 (2009).
147. A. V. Prokopiev, V. B. Ershova, O. Anfinson, D. Stockli, J. Powell, A. K. Khudoley, D. A. Vasiliev, N. N. Sobolev, and E. O. Petrov, “Tectonics of the New Siberian Islands archipelago: Structural styles and low temperature thermochronology,” *J. Geodynam.* **121**, 155–184 (2018).
148. A. Prokopiev, A. Khudoley, A. Egorov, M. Gertseva, E. Afanasieva, A. Sergeenko, V. Ershova, and D. Vasiliev, “Late Cretaceous–Early Cenozoic indicators of continental extension on the Laptev Sea shore (North Verkhoyansk),” in *Proceedings of “3P Arctic”* (Stavanger, Norway, October 14–18, 2013).
149. P. W. Reiners and M. T. Brandon, “Using thermochronology to understand orogenic erosion, *Ann. Rev. Earth Planet. Sci.* **34**, 419–466 (2006).
<https://doi.org/10.1146/annurev.earth.34.031405.125202>
150. B. D. Ricketts, “New Formations in the Eureka Sound Group, Canadian Arctic Islands,” *Geol. Surv. Can., Curr. Res.: Part B, Pap.* 86–01B, 363–374 (1986).
151. W. R. Roest and S. P. Srivastava, “Sea-floor spreading in the Labrador Sea: A new reconstruction,” *Geology* **17** (11), 1000–1003 (1989).
[https://doi.org/10.1130/0091-7613\(1989\)017<1000:SFS-ITL>2.3.CO;2](https://doi.org/10.1130/0091-7613(1989)017<1000:SFS-ITL>2.3.CO;2)
152. M. Seton, R. D. Müller, S. Zahirovic, C. Gaina, T. Torsvik, G. Shephard, et al., “Global continental and ocean basin reconstructions since 200 Ma,” *Earth Sci. Rev.* **113** (3–4), 212–270 (2012).
<https://doi.org/10.1016/j.earscirev.2012.03.002>
153. G. E. Shephard, R. D. Müller, and M. Seton, “The tectonic evolution of the Arctic since Pangea breakup: Integrating constraints from surface geology and geophysics with mantle structure,” *Earth Sci. Rev.* **124**, 148–183 (2013).
<https://doi.org/10.1016/j.earscirev.2013.05.012>
154. S. Skolotnev, G. Aleksandrova, T. Isakov, T. Tolmacheva, A. Kurilenko, E. Raevskaya, S. Rozhnov, E. Petrov, and A. Korniyuchuk, “Fossils from seabed bedrocks: Implications for the nature of the acoustic basement of the Mendeleev Rise (Arctic Ocean),” *Mar. Geol.* **407**, 148–163 (2019).
<https://doi.org/10.1016/j.margeo.2018.11.002>
155. R. A. Stephenson, A. F. Embry, S. M. Nakiboglu, and M. A. Hastaoglu, “Rift-initiated Permian to Early Cretaceous subsidence of the Sverdrup Basin,” *Sedimentary Basins and Basin-Forming Mechanisms*, Ed. by C. Beaumont and A. J. Tankard (Atlantic Geosci. Soc. Spec. Publ., 1987, Vol. 5), pp. 213–231.
156. M. Talwani and O. Eldholm, “Evolution of the Norwegian–Greenland Sea,” *Bull. Geol. Soc. Am.* **88**, 969–999 (1977).
157. J. A. Tarduno, D. B. Brinkman, P. R. Renne, R. D. Cottrell, H. Scher, and P. Castillo, “Evidence for extreme climatic warmth from Late Cretaceous arctic vertebrates,” *Science* **282**, 2241–2243 (1998).
158. F. Tessensohn and K. Piejohn, “Eocene compressive deformation in Arctic Canada, North Greenland and Svalbard and its plate tectonic causes,” *Polarforschung* **68**, 121–124 (2000).
159. R. Thorsteinsson and E. T. Tozer, “Geology of the Arctic Archipelago,” in *Geology and Economic Minerals of Canada*, Ed. by R. J. W. Douglass (Geol. Surv. Can. Econ. Geol. Rep. 1970, Vol. 1), pp. 547–590.
160. T. H. Torsvik, B. Steinberger, G. E. Shephard, P. V. Doubrovine, C. Gaina, M. Domeier, et al., “Pacific–Panthalassic reconstructions: Overview, errata and the way forward,” *Geochem., Geophys., Geosyst.* (G_3) **20**, 3659–3689 (2019).
<https://doi.org/10.1029/2019GC008402>
161. H. P. Trettin, “The Arctic Islands,” in *The Geology of North America, An Overview*, Ed. by A. W. Bally and A. R. Palmer (GSA, 1989, Vol. A, Ch.13), pp. 349–370.
162. N. A. Van Wagoner, M.-C. Williamson, P. T. Robinson, and I. L. Gibson, “First samples of acoustic basement recovered from the Alpha Ridge, Arctic Ocean: New constraints for the origin of the ridge,” *J. Geodynam.* **6**, 177–196 (1986).

163. M. Villeneuve and M.-C. Williamson, “ $^{40}\text{Ar}/^{39}\text{Ar}$ dating of mafic magmatism from the Sverdrup Basin Magmatic Province,” in *Proceedings of the 4th International Conference on Arctic Margins (ICAM IV)*, Ed. by R. A. Scott and D. K. Thurston (Anchorage, Alaska, USA, 2006), pp. 206–215.
164. P. Wessel and L. W. Kroenke, “Pacific absolute plate motion since 145 Ma: An assessment of the fixed hot spot hypothesis,” *J. Geophys. Res.* **113**, B06101 (2008). <https://doi.org/10.1029/2007JB005499>
165. M.-C. Williamson, D. Kellett, D. Miggins, A. Koppers, R. Carey, G. Oakey, D. Weis, W. Jokat, and E. Massey, “Age and eruptive style of volcanic rocks dredged from the Alpha Ridge, Arctic Ocean,” in *EGU General Assembly, 2019. Geophys. Res. Abstracts* (Vienna, 2019), Vol. 21, EGU2019-6336.
166. R. C. Whittaker, N. E. Hamann, and T. C. R. Pulvertaft, “A new frontier province offshore northern West Greenland: Structure, basin development and petroleum potential of the Melville Bay area,” *AAPG Bull.* **81**, 979–998 (1997).
167. D. Worsley, T. Agdestein, J. G. Gjelberg, K. Kirkemo, A. Mørk, I. Nilsson, S. Olaussen, R. J. Steel, and L. Stemmerik, “The geological evolution of Bjørnøya, Arctic Norway: Implications for the Barents Shelf,” *Norw. J. Geol.* **81**, 195–234 (2001).

Publisher’s Note. Pleiades Publishing remains neutral with regard to jurisdictional claims in published maps and institutional affiliations. AI tools may have been used in the translation or editing of this article.